Magnetotelluric theory and practice in geothermal exploration

Wouter van Leeuwen[1] and dr. Yunus Daud[2]
1. IF Technology, 2. University of Indonesia, 2016
Course developed for GEOCAP

Magnetotelluric theory and practice in geothermal exploration
Reader, IF Technology bv
Developed for GEOCAP

Coverphoto: Carlo Lodigiani, Gunung Lawu, 15-06-2015.
Lay-out: LaTeX

Contents

1

Theory and practice of the magnetotelluric method in geothermal exploration

1.1 Introduction

Magnetotellurics is a non-evasive geophysical technique which utilizes the variations in the Earth's electromagnetic field to image the electrical resistivity structure of the subsurface. The magnetotelluric method is utilized for research purposes and commercial activities such as deep crustal studies, exploration for mining and offshore hydrocarbon. In addition to these applications, magnetotellurics has a long track record in the exploration of convection-dominated play type geothermal systems[1] and particularly volcanic type geothermal systems, which have a clear signature in resistivity models.

In this course an introduction is given to the most important theory and assumptions used for the magnetotelluric method. In this Section questions such as *"what are we measuring?"*, *"what do we see on the screen?"*, and *"how can we use magnetotellurics in geothermal exploration?"* are addressed. The theoretical basis is expanded on in Section 1.6.

In Section 1.7 common causes of effects on the measured magnetotelluric data are discussed, as are several mitigation measures for these effects. A good-practice field procedure addressing key factors during data acquisition is presented in Section 1.11. In these two Sections questions such as *"How do we recognize errors or faulty data?"*, as well as a strategy to assess the quality of a magnetotelluric data set, are addressed. The next Section 1.12 discusses the main theoretical principles of magnetotelluric data processing theory.

In Sections 1.13 and 1.14 inversion and interpretation of the subsurface models derived from magnetotelluric data are discussed. Here attention will be paid to questions such as *"Do I see geology or a model artefact?" and "How do I recognize my geothermal reservoir?"* are addressed.

The learning outcomes, listed by complexity, achieved by the students by end of this course are:

1. The students can recall the basic electromagnetic principles.
2. The students can name the properties of the magnetotelluric transfer function.
3. The students can identify the main causes of distortion of the magnetotelluric signal.
4. The students can recall the basic concepts of magnetotelluric data processing and inversion.
5. The students can describe the (field) procedures to maximize magnetotelluric data quality before and during data acquisition.

[1] See Section 1.4 for details

6. The students can discuss the basic concepts of the tools and techniques available for magnetotelluric data quality assurance (QA) and quality check (QC).
7. The students can determine if a magnetotelluric field survey is properly designed and carried out.
8. The students can QC the delivered magnetotelluric stations responses.
9. The students can run 1-D and 2-D inversions of a magnetotelluric data set and interpret the results.
10. The students can assess the quality of a resistivity model and its geothermal interpretation.

It is the intention of this course that the participants are, after the successful completion of the course, able to explain others the the main principles of the magnetotelluric method. Furthermore, they will know how to carry out magnetotelluric fieldwork or modelling for geothermal prospecting and transfer this knowledge to others. To some extent, the participants will also be able to carry out a quality check on acquired magnetotelluric data as well as assess the validity, reliability and accuracy of any resistivity model and its interpretation made on the basis of magnetotelluric data.

Parts of this Chapter are derived and/or modified from the Thesis of *van Leeuwen* [2016].

1.2 Geothermal energy

The International Geothermal Association (IGA) defines geothermal energy as "that part of the Earth's heat that can, or could be, recovered and exploited by man" [*Dickson and Fanelli*, 2004]. It is this definition that will be used in this reader from now on when referring to geothermal energy.

Radiogenic heat production in the mantle and crust is the main source of Earth's heat. Other sources contributing to the Earth's surface heat flow are the Earth's core and mantle cooling. The Earth's heat is conducting through the mantle to be stored in rocks and/or water in the crust. It is the utilization of this thermal energy, present in liquid water or as trapped steam within(porous) rocks and in the rocks itself, that we are after.

A geothermal system is defined by *Williams et al.* [2011] as "any localized geological setting where portions of the Earth's thermal energy may be extracted from natural or artificially induced circulating fluids transported to a point of use." Geothermal systems are conventionally classified in terms of their temperature, leaving the geological setting, reservoir parameters like porosity and permeability as well as economic viability of the system out of the classification.

Inspired by hydrocarbon exploration and considering the above, *Moeck* [2014] suggested to categorize geothermal systems by play type. The definition of a geothermal play is the model which comprises the geological factors controlling a technically and economically recoverable geothermal resource [*Moeck*, 2013]. These geological factors must provide the heat source, the reservoir, the heat or fluid pathways, the seal of the reservoir, the storage capacity of the play, and the potential for economic recovery of the heat [*Moeck*, 2013, 2014].

Geothermal plays are divided into conduction-dominated type plays and convection-dominated type plays [*Moeck*, 2014]. Here, conduction and convection are related to the dominant mechanism of heat transfer providing the geothermal system's heat source. In geothermal, conduction is the transfer of heat between geological formations that are in direct contact with each other. In other words, the heat is transferred to the Earth's surface through solid rocks. Convection in geothermal is the circular process of a hot liquid or gas rising towards the surface, after which a cooler liquid or gas takes its places and is heated again. Generally said, the heat is transferred in the geothermal reservoir via liquids or gas.

Convection-dominated type plays are related to recent, i.e. less than roughly one million years old, volcanic activity found near plate boundaries like subduction zones (the "Ring of Fire" in the Pacific), continental rifts (East African Rift), mid-ocean ridges and transform fault spreading, or at hot spot anomalies (Hawaii, Iceland). Conductive type plays are for example found in areas with an increased heat flow in the continental crust often generated by radioactive isotope decay, hot water percolating upward along fault zones, or deep seated intrusive bodies, see Figure 1.1.

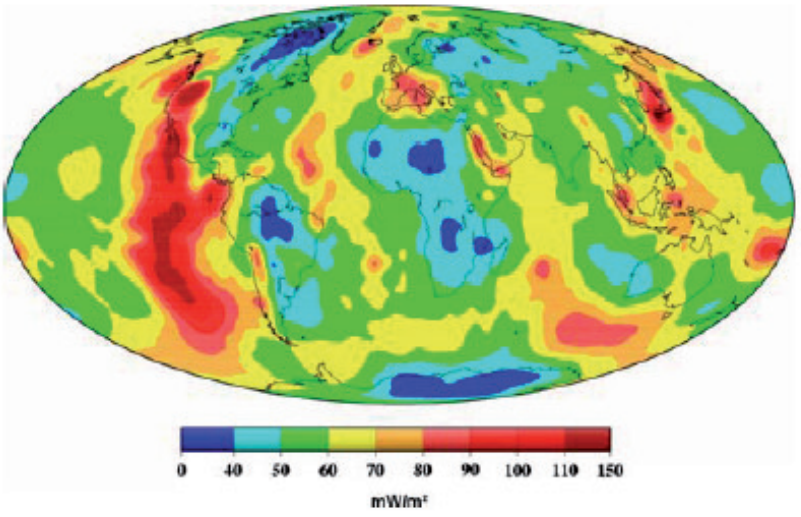

Figure 1.1: Global surface heat flow map.

After drilling the first exploration well, geothermal plays are geologically described by their conceptual model. A conceptual model is defined as the geological model, both descriptive and graphic, containing the relevant structures and processed that determine the geothermal reservoir and it's response to exploitation [*Grant and Bixley*, 1982; *Axelsson*, 2013]. The conceptual model of each geothermal play type is defined by a number of geological factors which need to be known before the geothermal system can be developed. The exploration plan of a geothermal play should be designed to determine these factors a accurate as possible. Depending on the geology of the geothermal system considered, different exploration techniques might be necessary. Although the characteristics of the various geothermal play types are different, they consist of the same elements together defining it's conceptual model.

1. The heat source, (continuously) providing the system with geothermal energy.
2. The geothermal reservoir, containing the recoverable geothermal energy of the system.
3. The seal or cap rock trapping the geothermal energy (or it's agent) in the reservoir.

Logically the way these three geological factors are formed throughout geological history and their relation is a key part of the conceptual model. Besides these geological factors, the temperatures, permeability depth and dimensions of (the liquid or gas in) the geothermal reservoir are needed to estimate the total amount of energy it contains as well as it's economic viability.

Geothermal energy is utilized for electrical power generation or for direct heat applications. The advantages of electrical power generation from geothermal energy are apparent when connected to the electrical grid or on remote locations with insufficient power supply including isolated islands, areas with a high energy demand (industrial processes, mining) or there where other energy sources are scarce or expensive. Finally, it is one of the many sustainable energy alternatives alongside e.g. wind, solar, and hydro. Geothermal energy can be utilized as direct heat for industrial purposes for those industrial processes needing high temperatures such as the paper industry or aluminium production. This type of exploitation of geothermal heat, without the use of ground source heat pumps, is referred to as direct heat. Direct heat is also applied for the heating of residential buildings and offices as well as utility buildings, often via a district heating system. Another known direct heat application is the heating of greenhouses by geothermal energy, although in those cases a ground source heat pump is generally installed and the term direct use is more appropriate.

1.3 Factors affecting geological resistivity

1.3.1 Resistivity

The electrical resistivity ρ is defined through Ohm's law, which states that the electrical field strength E (V/m) is proportional to the current density j (A/m^2)

$$E = \rho j. \tag{1.1}$$

In Equation 1.1 the proportional constant, the electrical resistivity ρ (Ωm), depends on the material. The reciprocal of resistivity is conductivity σ (S/m). The electrical resistivity can also be defined as the ratio of the potential difference $\triangle V$ (V/m) to the current I (A)

$$\rho \approx \frac{\triangle V}{I}. \tag{1.2}$$

1.3.2 Conduction mechanisms

There are several conduction mechanisms possible in Earth materials. These mechanisms are:

- Electronic conduction occurs in pure metals. The charge carriers in the case of electronic conduction are electrons that exist as a gas between ions and can move easily through the metal. As a consequence, the resistivity of metals is very low ($\tilde{}$ $1.6{\cdot}10^{-8}\Omega$m).
- Semiconduction occurs in minerals such as sulphides which are typically found in igneous rock. The charge carriers in the case of semiconduction are electrons, ions or holes. Compared to metals, the resistivity is usually higher (typically 10^{-3} to $10^{-5}\Omega$m). Semiconduction usually shows a temperature dependence.
- Ionic conduction in brines occurs as the ions can freely move in liquid (either aqueous fluids or molten materials). As the salinity of a brine increases, the resistivity decreases as more charge carriers become available.

1.3.3 Geological resistivity

The resistivity of Earth materials is controlled by the following factors.

Melt At temperatures above 800 °C, magma itself has a very low intrinsic resistivity. The resistivity of the melt is greatly dependent on the melt composition, the fraction of partial melt and the presence of water in the melt.

Hydrothermal clay alteration Also affecting the electrical resistivity of a geothermal system is its hydrothermal clay alteration mineralogy. Hydrothermal clay alteration occurs when hydrothermal fluids in a geothermal system interact with the volcanic (basaltic or acidic) host rocks. As explained in the caption of Figure 1.2, temperature is the most important parameter controlling the clay mineralogy of a geothermal system. In the presence of clay alteration, an extra conduction pathway along the interface of clay minerals, as shown in Figure 1.2, is formed. Alteration mineralogy is a reflection of the maximum temperature experienced by the rocks while the actual temperature might be lower.

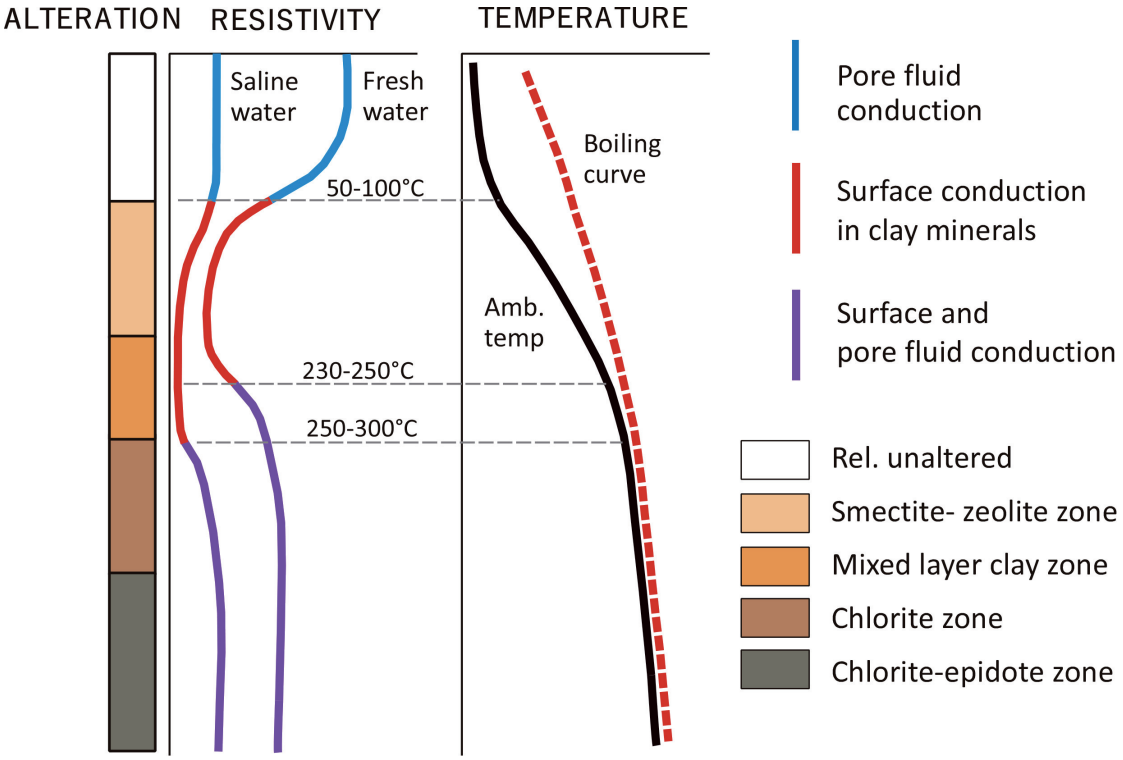

Figure 1.2: Generalized depth-conductivity and depth-temperature structure of a basaltic geothermal system. From *Flóvenz et al.* [2005]. At different temperature regimes, specific clay alteration minerals are formed in the subsurface often forming a impermeable clay cap covering the geothermal reservoir. At temperatures above 70 °C these minerals are smectite and zeolites having a high electrical conductivity. At temperatures between 180 °C and 220-240 °C a mixture of these clay minerals with illite, in acidic regimes, and/or chlorite, in basaltic regimes, are found. These newly formed clay alteration minerals tend to reduce the conductivity. Above 240 °C the smectite has completely disappeared and a pure cholorite or illite zone is formed and bulk conductivity is increasing again. At even higher temperatures epidote is added to the alteration mineralogy.

Porosity and permeability Another factor affecting the resistivity of rock is the porosity and permeability. The dependency between electrical resistivity and porosity is given in empirical relations such as *Archie* [1942].

$$\frac{\rho_0}{\rho_w} = \phi^{-m} S_w^{-n} \tag{1.3}$$

where ρ_0 and ρ_w are the electrical resistivity of the rock and the water, ϕ is the porosity, m is the cementation factor, S_w is the water saturation, and n is the saturation exponent.

The saturation, i.e. the fraction of fluid present in the pore space, also effects the electrical resistivity of a porous rock. When filled with water, the higher the saturation, the lower the resistivity. As temperature increases (with depth), the resistivity of fluids decreases and the bulk electrical resistivity decreases as well. With increasing pressure (with depth), porosity and permeability are decreasing and therefore bulk electrical resistivity increases.

Fluid composition The hot fluids flowing upwards from the contact between the groundwater and magma influence the resistivity of the geothermal system. As the fluids present in rocks can contain varying concentrations of dissolved salts, the fluid salinity also plays a role in the electrical resistivity response of the subsurface. Fluids having a higher concentration of dissolved salts generally have a higher conductivity.

Given the factors influencing the electrical resistivity of the subsurface, relationships are being investigated and developed to predict rock temperature, porosity and permeability or clay alteration mineralogy directly or indirectly from resistivity measurements. In addition to predicting the temperature, the alteration mineralogy is often utilized for the structural interpretation of geothermal systems.

1.4 Magnetotellurics in geothermal exploration

The previous Section lists the factors affecting the bulk electrical resistivity of the subsurface and more specifically geothermal systems. Utilizing this knowledge, the resistivity characteristics for geothermal exploration of the various geothermal systems can be illustrated on the basis of a selection of case studies. Two review papers, discussing the geothermal application of the magnetotelluric method based on case studies, were published by *Spichak* [2009] and *Muñoz et al.* [2010]. In this Section the classification of geothermal systems based on play types uses the play-type definitions of *Moeck* [2014].

Convection-dominated geothermal play types

A volcanic type geothermal system consists of a fluid upflow area overlain by a clay-cap. As discussed in Section 1.3, this clay-cap consists of clay alteration minerals such as smectite and illite. The electrical resistivity structure consisting of a highly conductive layer located above an *up-doming* zone, with a relatively lower conductivity, is a characteristic electrical response for a volcanic type geothermal system. The fluid upflow area is caused by thermal buoyancy through the permeable reservoir and is characterized by an up-doming pattern of isotherms simultaneously reflecting the pattern of fluid flow. This generalized concept of the electrical resistivity structure of a volcanic type geothermal play is illustrated in Figure 1.3. It is inferred that the base of the clay-cap coincides with a temperature contour of the geothermal reservoir often assumed as around 220°C. Since the hot geothermal fluids flow laterally away from the upflow zone, the clay-cap may thicken in the outflow zone.

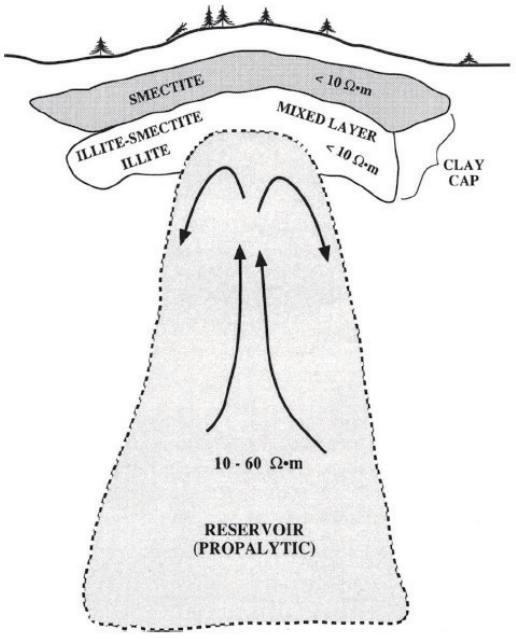

Figure 1.3: Generalized electrical resistivity model of a volcanic type geothermal system with a reservoir temperature of above 200 °C. From *Pellerin et al.* [1996].

Application of magnetotellurics for the exploration of these types of geothermal systems is common and often successful. The generalized resistivity model described above can be applied successfully to the survey results, particularly when the volcanic system is active. A characteristic example of the successful application of this resistivity model of a volcanic geothermal play type is the Taupo Volcanic zone in New Zealand [*Bibby et al.*, 1995; *Heise et al.*, 2008], see Figure 1.4, as well as the Hengill area in Iceland [*Árnason et al.*, 2010], see Figure 1.5.

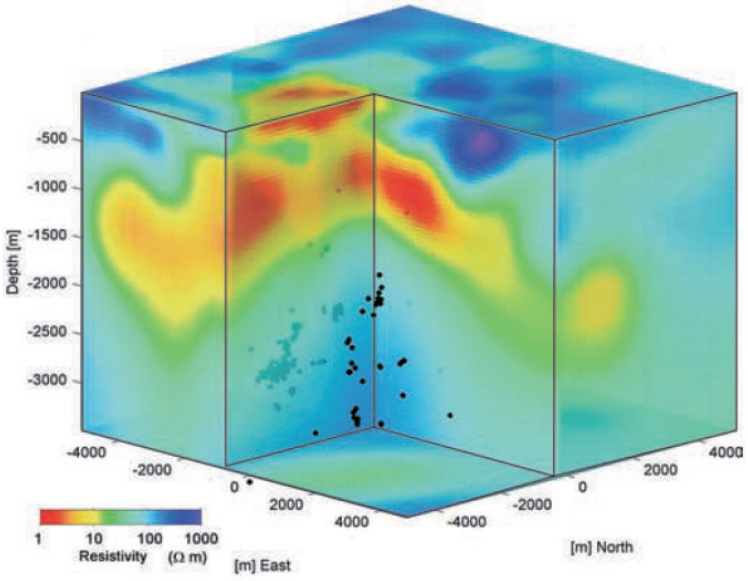

Figure 1.4: 3-D view of resistivity from inversion modelling results of the Taupo volcanic zone. Earthquake locations are shown as black dots. The highly conductive zone is the clay cap consisting of hydrothermal alteration minerals, while the geothermal reservoir can be recognized by the more resistive area below. See *Heise et al.* [2008] for details.

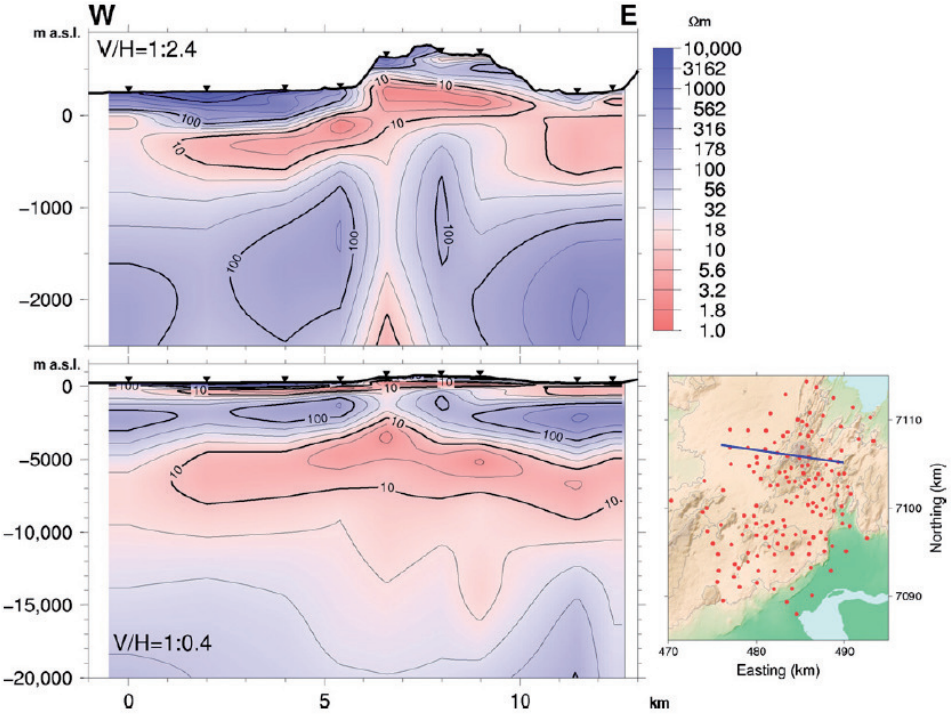

Figure 1.5: West-east resistivity cross-sections across the Hengill geothermal area for two different depth ranges obtained from stitched 1-D inversion models. Inverted triangles are magnetotelluric stations and V/H is the ratio between the vertical and the horizontal axis scales. The location of the cross-section is shown in the map on the right in which the red dots are magnetotelluric stations. In the shallow cross section the conductive clay cap and the more resistivity geothermal reservoir can be recognized. The conductive heat source is observed in the deep cross section. See *Árnason et al.* [2010] for details.

In contrast to the Hengill area, the Krýsuvík geothermal system, also in Iceland located, has no central volcano and the retrieved 3-D resistivity model can not be interpreted similarly. Although the Krýsuvík geothermal system is characterized by the typical resistivity-depth profile related to hydrothermal alteration found in Iceland, its deep conductor is not related to a fluid upflow zone, but probably the result of inflation due to the emission of gas [*Hersir et al.*, 2013], see Figure 1.6. Here, recovered temperatures are lower than the clay alteration mineralogy suggests, indicating that cooling has taken place.

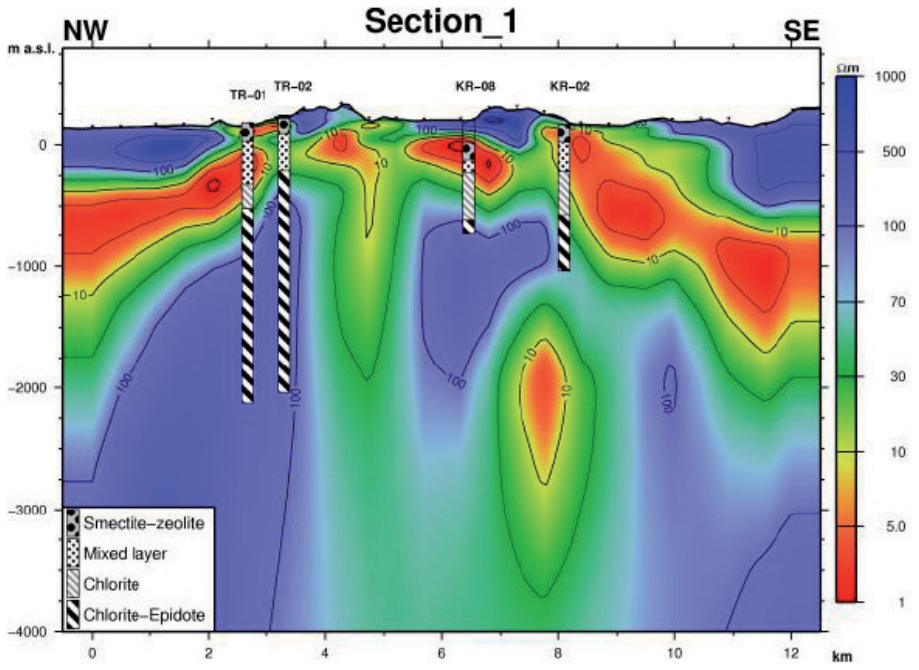

Figure 1.6: Resistivity cross section of the Krýsuvík geothermal system. Although a conductive clay cap and a more resistive reservoir can be identified, the geological interpretation is not as straight forward. The conductive structure at 2,000 m depth located at 8 km distance in this cross section is probably related to the emission of gas. See *Hersir et al.* [2013] for details.

An example of the geothermal exploration of a plutonic type geothermal play is given by the case of the Travale geothermal system situated in Tuscany, Italy. The Travele geothermal system is heated by a deep-seeted pluton, while the fluid flow is fault-controlled, see Figure 1.7. Low resistivity zones in the inversion model of the geothermal system are coincident with high permeability and porosity and possibly also hydrothermal clay alteration. This geothermal system has two producing reservoirs, a shallow fractured metamorphic formation and a deeper porous limestone formation, both characterized by reduced resistivities [*Manzella et al.*, 2006].

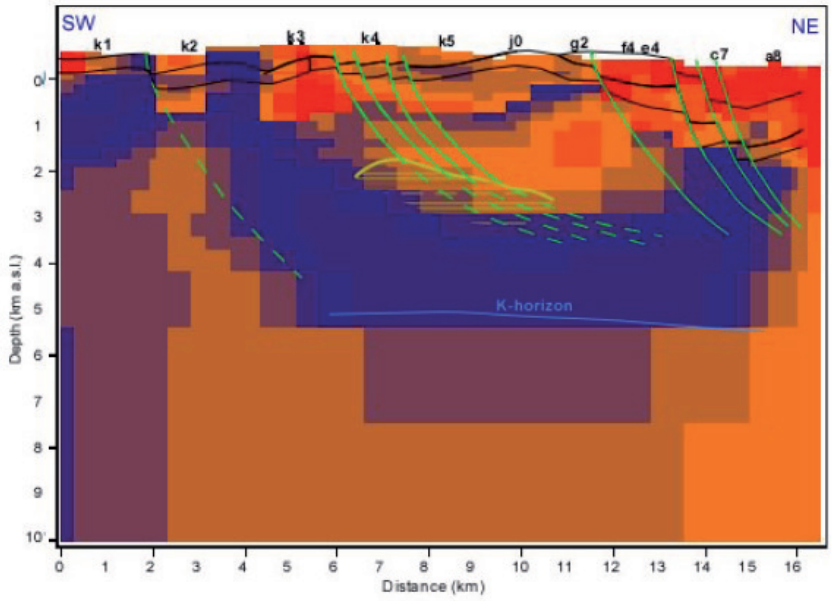

Figure 1.7: 2-D Resistivity inversion model with overlapping geology of the Travale geothermal field. Faults are plotted as green lines, while black lines are seismic reflections. Red is a low resistivity while blue is a high resistivity. The low resistivity zones are inferred to be porosity and permeability controlled geothermal reservoirs. See *Manzella et al.* [2006] for details.

The Coso geothermal field in the western United States is an example of a geothermal system fitting an extensional-domain play type. The geothermal field is characterized by a deep magma reservoir which is slowly moving upwards. The lava intrusions into the basement rocks beneath the geothermal reservoir are derived from this magma reservoir. The geothermal reservoir permeability is fracture controlled [*Wannamaker et al.*, 2005]. The 3-D resistivity model of the Coso geothermal field shows a steeply dipping low resistivity zone which is related to the fluid flow in the main fault in the field, see Figure 1.8. This leads to the conclusion that this geothermal system is both temperature and porosity and permeability controlled. The shallow resistivity layers of the system are also characterized by the typical resistivities associated with hydrothermal alteration [*Newman et al.*, 2008].

In summary, it is observed that all geothermal play types in convection-dominated geothermal systems have, due to their high temperatures, generally a resistivity imprint from hydrothermal alteration mineralogy. However, when geothermal systems are fracture or porosity and permeability controlled, low resistivity anomalies are often related to the controlling geological structures instead of alteration mineralogy.

Conduction-dominated geothermal play types

For conduction-dominated type geothermal systems, the associated resistivity structure is often dominated by the porosity and permeability of the geological structures,

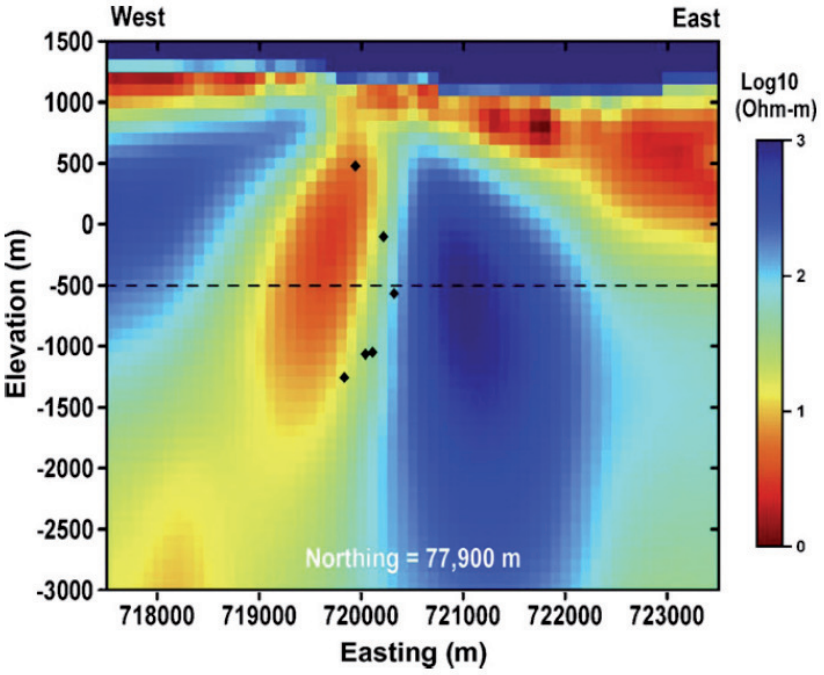

Figure 1.8: West-east orientated resistivity cross section of the Coso goethermal field. Major drilling mud losses, interpreted to be fracture related, are shown by black diamonds. The very low resistivity in this area is interpreted as a fractured permeable zone which controls the resistivity. The shallow low resistivity layer is the clay cap of alteration minerals. See *Newman et al.* [2008] for details.

although temperature and alteration mineralogy might play a role as well. These systems are generally located in stable tectonic regions with thick sedimentary sequences. In many of these cases resistivity imaging as sole geophysical method does not sufficiently distinguish the layered sediments, and other geophysical methods such as seismics, which do not detect directly permeability or temperature, are often utilized as well.

Examples of conduction-dominated geothermal systems can be found at Groß-Schönebeck in Germany and at Skierniewice in Poland, both located in an intracratonic basin type geothermal play. In Groß-Schönebeck a joint interpretation of magnetotelluric and seismic data was carried out to accurately interpret the geology of the site. As shown in Figure 1.9, the targeted reservoir formations are deep sandstones and volcanic strata hosting aquifers, heated by a granitic intrusive body. Low resistivity structures in this geological setting are related to fracture anhydrites, resulting in enhanced permeability [*Muñoz et al.*, 2010; *Muñoz*, 2014]. The geology of the geothermal system at Skierniewice is purely sedimentary and consists of an at least 8 kilometres thick sedimentary succession. Using a combination of magnetotelluric and seismic data *Bujakowski et al.* [2010] were able to identify permeable structures coinciding with fractured zones in the subsurface.

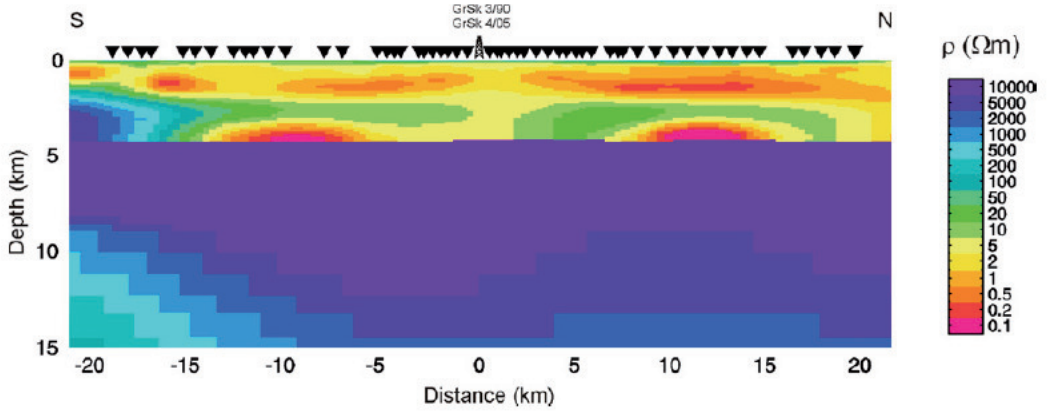

Figure 1.9: Electrical resistivity model obtained from the inversion of magnetotelluric data using a high-resistivity basin floor from a seismic velocity model as a priori information. The inverted triangles are magnetotelluric stations. The shallow resistive sedimentary layers are seen to overly a thick sequence of evaporites, while the deep conductive anomalies are associated with fractures anhydrite. See *Muñoz et al.* [2010] for details.

As geothermal systems in an orogenic belt play type setting are generally located in small sedimentary basins, similar exploration strategies as used for intracratonic basin type plays are utilized. The Llucmajor aquifer system as shown in Figure 1.10 is an example of such a system. Here magnetotellurics is used to identify two moderately resistive aquifers (R1 and R2 in Figure 1.10, one shallow unconfined and the other deeper and confined, as well as a conductive aquitard (C in Figure 1.10) separating the two aquifers in the geothermal system. This system is conceptualized by a lower reservoir containing the thermal waters and a fault allowing the vertical flow of waters where the aquitard is thinnest [*Arango et al.*, 2009].

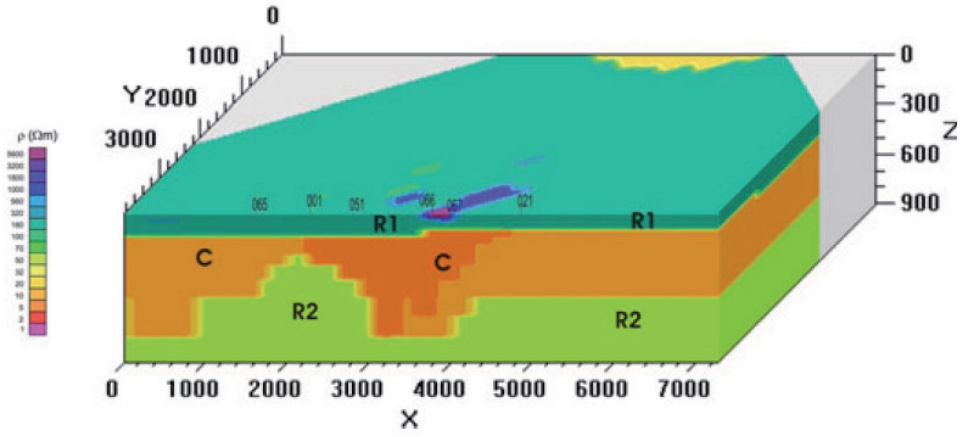

Figure 1.10: A "trial and error" forward 3-D resistivity model of the Llucmajor aquifer system. The shallow and deep aquifers correspond with the regions with moderate resistivity, while the confining aquitard corresponds with low resistivity [*Muñoz*, 2014; *Arango et al.*, 2009].

Finally, as basement geothermal play types tend to target very high temperatures, volcanic influences are often present and alteration mineralogy can play a role in the resistivity models of these systems. This can be seen at the geothermal test site of Soulz-sous-Forêts, France, targeting a granite. Here a resistivity model was developed reconstructing the graben including the faults in which it is located. The low resistivities in this model are attributed to either clay alteration minerals or pore-space [*Geiermann and Schill*, 2010]. Another example of a basement play type geothermal system is the Habanero Geothermal EGS Project, where a 2-D resistivity model was developed (Figure 1.11). Situated in a stable craton this model is characterized by three layers, with low resistivities up to 2 kilometre depth for unconsolidated sediments, intermediate resistivities for consolidated sediments between 2 and 4 kilometre depth and high resistivities for the granitic basement at depths greater than 4 kilometre [*Didana et al.*, 2015], as shown in Figure 1.11.

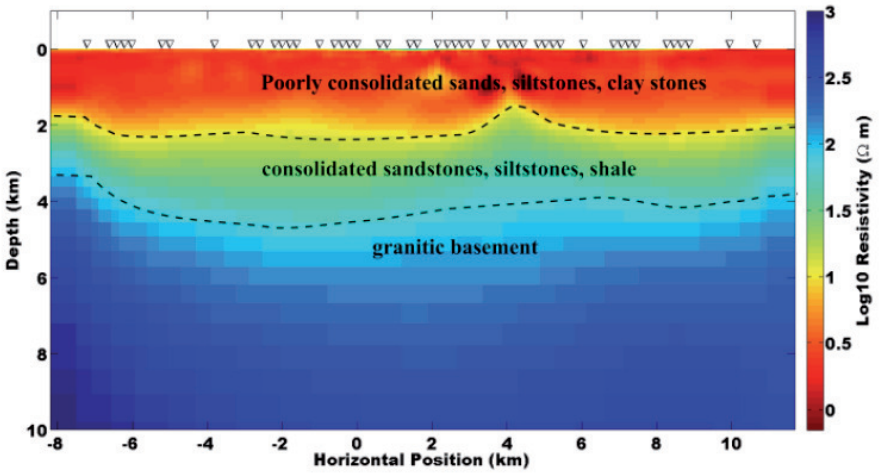

Figure 1.11: 2-D resistivity inversion model of the Habanero Geothermal EGS project showing the three resistivity layers corresponding with geological formations. Inverted triangles are magnetotelluric measurements. From *Didana et al.* [2015].

1.5 Electromagnetic principles

During a magnetotelluric experiment, the time-variations in the electromagnetic field of the Earth are measured in order to determine the electrical resistivity structure of the subsurface. These electromagnetic field variations are mainly caused by external source phenomena such as magnetic storms and lighting activity and by geological variations. Magnetic storms are time-variations in the solar wind, whose deflection by the Earth's internal magnetic field creates the magnetosphere as illus-

trated in Figure 1.12. In Figure 1.12 a diagram of the magnetosphere is sketched. The time-variations in the solar wind can induce large electric currents in the ionosphere which in turn produce large changes in the magnetic field at the Earth's surface at frequencies below 1 Hz. The time-variations in the Earth's electromagnetic field with frequencies above 1 Hz are caused by worldwide lighting activity.

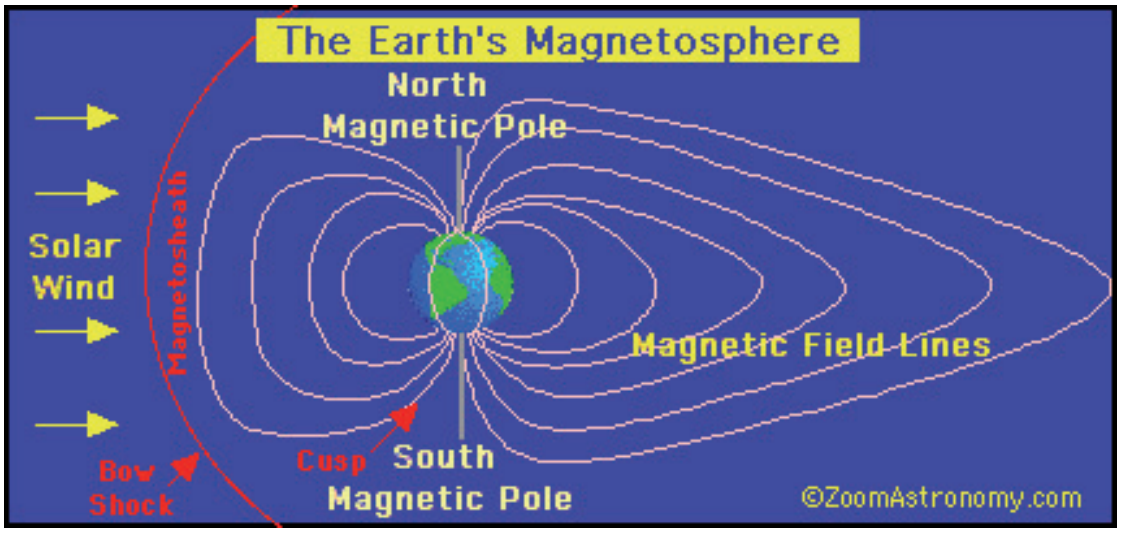

Figure 1.12: Diagram of the Earth's magnetosphere.

The principles of magnetotellurics were first published by *Rikitake* [1948], *Tikhonov* [1950] and *Cagniard* [1953]. They realized that the electric response of the Earth could be obtained from large depths by extending the measuring (or sounding) period during a magnetotelluric experiment. This principle is described in the electromagnetic skin depth relation, which is in a simplified form:

$$p(T) \approx 500\sqrt{T\rho_a}, \tag{1.4}$$

Here $p(T)$ is the electromagnetic skin depth in metres (m), T is the magnetotelluric sounding period in seconds (s) and ρ_a is the apparent bulk resistivity of the subsurface in Ohm-metre (Ωm).

Bulk electrical resistivity of Earth's materials in the crust and upper mantle range from 10^{-1} to 10^5 Ωm. Magnetotelluric experiments are typically conducted in the frequency range from 10^{-5} to 10^5 s. Consequently, the skin depth of a magnetotelluric experiment ranges from several tens of meters to several hundreds of kilometres, or in other words from the near-surface to deep into the Earth's mantle.

The relationship between electrical and magnetic fields in a medium is described by the Maxwell equations.

1. Faraday's law of magnetic induction:

$$\nabla \times \boldsymbol{E} = -\frac{\partial \boldsymbol{B}}{\partial t} \tag{1.5}$$

2. Ampere's law:

$$\nabla \times \boldsymbol{H} = \boldsymbol{j}_f + \frac{\partial \boldsymbol{D}}{\partial t} \tag{1.6}$$

3. Gauss' law for magnetic fields:

$$\nabla \cdot \boldsymbol{B} = 0 \tag{1.7}$$

4. Gauss' law for electric fields:

$$\nabla \cdot \boldsymbol{D} = \eta_f \tag{1.8}$$

where $\boldsymbol{E}$ is the electric field in volt per metre (Vm^{-1}), $\boldsymbol{B}$ is the magnetic induction in tesla (T), $\boldsymbol{H}$ is the magnetic intensity in ampere per metre (Am^{-1}), $\boldsymbol{D}$ is the electric displacement in coulomb per square metre (Cm^{-2}), $\boldsymbol{j}_f$ is the electric current density in ampere per square metre (Am^{-2}), and η_f the electric charge density in coulomb per cubic metre (Cm^{-3}).

Assuming linear constitutive relationships in the material properties of the medium and considering that time-varying displacements currents are negligible, electric and magnetic fields can be related through the constitutive equations

$$\boldsymbol{j}_f = \sigma \boldsymbol{E} \tag{1.9}$$

$$\boldsymbol{D} = \varepsilon \boldsymbol{E} \tag{1.10}$$

$$\boldsymbol{B} = \mu \boldsymbol{H} \tag{1.11}$$

where σ is the electrical conductivity in siemens per metre (Sm^{-1}), ε is the electrical permittivity in farads per metre (Fm^{-1}), and μ is the magnetic permeability in henries per metre (Hm^{-1}).

Furthermore, considering an isotropic medium, i.e., where electric permittivity ε and electrical conductivity σ are all scalars, as well as assuming a free space magnetic permeability η_0, a set of Maxwell equations becomes available which can be used for a wide range of geophysical problems including magnetotelluric .

1.6 The Magnetotelluric transfer function

In Section 1.5 a quick tour is made through the principal concepts of the magnetotelluric method. In this Section it is explained how the measured electric and magnetic fields are related via the *magnetotelluric transfer function* $\overline{Z}$. Some practical properties of the magnetotelluric transfer function in relation to geothermal exploration are discussed as well.

Assuming a time-varying quasi-uniform horizontal magnetic field above the surface of the Earth, inducing an electric field within the Earth, the relation between the electric and magnetic fields at the surface of the Earth can be described by

$$\boldsymbol{E}_h = \overline{\boldsymbol{Z}} \cdot \boldsymbol{B}_h \tag{1.12}$$

where $\boldsymbol{E}_h$ and $\boldsymbol{B}_h$ are the horizontal electric and magnetic fields in the spectral domain. The magnetotelluric transfer function is the ultimate target during a magnetotelluric survey. It is estimated from the measured electric and magnetic fields.

A similar relationship between the horizontal and vertical magnetic fields can be formulated as

$$B_z = \boldsymbol{T} \cdot \boldsymbol{B}_h. \tag{1.13}$$

where B_z is the vertical magnetic field in the spectral domain and $\boldsymbol{T}$ is the vertical magnetic transfer function, or *Tipper*.

Taking the Maxwell equations describing the behaviour of electromagnetic fields in a polarisable, magnetisable medium as well as the constitutive equations, as given in Equations 1.5 to 1.11, the magnetotelluric transfer function can be derived.

For magnetotellurics it can be assumed that the Earth is isotropic and that the time-varying displacement currents and the variations in electrical permittivities ε and magnetic permeabilitities μ of the rocks are negligible compared to the variations in electrical resistivity. Following these assumptions Equations 1.6 to 1.8 can be reformulated to

$$\nabla \times \boldsymbol{B} = \mu_0 \sigma \boldsymbol{E} \tag{1.14}$$

$$\nabla \cdot \boldsymbol{E} = \eta_f / \varepsilon_0 \tag{1.15}$$

where μ_0 and ε_0 are respectively the free-space values of the magnetic permeability ($\mu_0 = 1.2566 \times 10^{-6}$ Hm^{-1}) and the electrical permittivity ($\varepsilon_0 = 8.85 \times 10^{12}$ Fm^{-1}). Furthermore, as displacement currents are negligible with respect to typical magnetotelluric sounding periods, the left hand side of Equation 1.14 can be set to zero. Assuming a homogeneous half-space and that no current sources exist within the Earth, Equation 1.15 can be set to zero as well.

According to Faraday's law (Equation 1.5) a time-varying primary magnetic field will induce a circulating electric field. This electrical field will, following Ampere's law (Equation 1.6), in turn induce a circulating secondary magnetic field with its axis directed perpendicular to the primary magnetic field. Assuming a plane wave, e.g. the incident magnetic field is planar, the electric and magnetic fields can be expressed as diffusive harmonic waves through the Earth. Since diffusion is a three-dimensional process, magnetotelluric soundings are in fact measuring volumetric averages of the Earth's material properties.

Using the assumptions discussed before and considering a layered Earth $\nabla \cdot \overline{\boldsymbol{E}} = 0$, implying that only horizontal electric fields are induced. Taking the curl of Equation 1.5 and applying this model yields

$$\nabla^2 \boldsymbol{E} = \mu_0 \sigma \frac{\partial \boldsymbol{E}}{\partial t} = i\omega\mu_0\sigma \boldsymbol{E}. \tag{1.16}$$

To arrive at the magnetotelluric transfer function an insulating uniform half-space at $z = 0$ is considered and Equation 1.5 for the x-component reduces to

$$\frac{\partial E_x}{\partial z} = -kE_x = -\frac{\partial B_y}{\partial t} = -i\omega B_y \tag{1.17}$$

in which $k_2 = i\omega\mu_0\sigma$. Equation 1.17 linearly relates the horizontal magnetic to the horizontal electric fields. This leads to the formulation of the magnetotelluric transfer function for the horizontal electric field in the x-direction and the horizontal magnetic field in the y-direction:

$$Z_{xy} = \frac{E_x}{B_y}. \tag{1.18}$$

Similarly equations can be derived for the relations between all horizontal electromagnetic field directions which leads to the definition of the magnetotelluric transfer function:

$$\begin{pmatrix} E_x \\ E_y \end{pmatrix} = \begin{pmatrix} Z_{xx} & Z_{xy} \\ Z_{yx} & Z_{yy} \end{pmatrix} \cdot \begin{pmatrix} B_x \\ B_y \end{pmatrix}. \tag{1.19}$$

Since in a 2-D case $Z_{xx} = Zyy = 0$ and considering Equations 1.17 to 1.19, the horizontal electric and magnetic fields for a uniform half-space can be related as

$$C = \frac{1}{k} = \frac{E_x}{i\omega B_y} = -\frac{E_y}{i\omega B_x}. \tag{1.20}$$

Here C is also known as the Smucker-Weidelt C-response. Knowing that the conductivity is the reciprocal of resistivity, the apparent resistivity ρ_a, as a function of frequency, can now be directly calculated from Equation 1.20

$$\rho_a = \frac{1}{\sigma} = \mu_0 \omega |C|^2. \tag{1.21}$$

Properties of the magnetotelluric transfer function

In addition to resistivity and phase, the magnetotelluric transfer function is known to have other properties containing information about the subsurface. Examples can be found in the TM-mode and TE-mode, the rotational invariants, as well as in the induction arrows.

TM-mode and TE-mode

The TM-mode and TE-mode can be described by considering a discontinuity in a 2-D Earth, for example a infinite vertically orientated discontinuity as illustrated in Figure 1.13. Since the current should be conserved across a discontinuity, the incident electric field E_y should also be discontinuous. All other fields are continuous and because there are no along-strike variations in the conductivity, the TM-mode (Equation 1.22) and TE-mode (Equation 1.23) are:

$$\left.\begin{aligned} \frac{\partial B_x}{\partial y} &= \mu_0 \sigma E_z \\ \frac{-\partial B_x}{\partial z} &= \mu_0 \sigma E_y \\ \frac{\partial E_z}{\partial y} - \frac{\partial E_y}{\partial z} &= i\omega B_x \end{aligned}\right\} \text{TM-mode.} \tag{1.22}$$

$$\left.\begin{aligned} \frac{\partial E_x}{\partial y} = \frac{\partial B_z}{\partial t} &= i\omega B_z \\ \frac{\partial E_x}{\partial z} = \frac{\partial B_y}{\partial t} &= -i\omega B_y \\ \frac{\partial B_z}{\partial y} - \frac{\partial B_y}{\partial z} &= \mu_0 \sigma E_x \end{aligned}\right\} \text{TE-mode.} \tag{1.23}$$

In the example with a vertical discontinuity of infinite length as shown in Figure 1.13, the TM-mode impedance, describing currents flowing perpendicular to the strike, is discontinuous at the conductivity discontinuity. Since the conductivity is not varying along the strike of the discontinuity the TE-mode impedance, describing currents flowing parallel to the strike, is continuous.

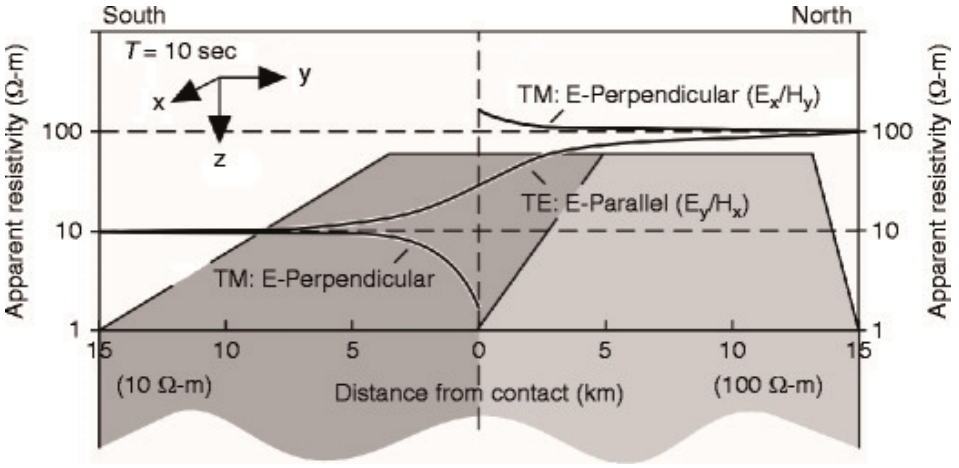

Figure 1.13: Apparent resistivity response of the TM-mode and TE-mode versus distance from a infinite vertical conductivity discontinuity (e.g., a fault plane).

Rotational invariants

The magnetotelluric transfer function $\overline{Z}$ maps $\boldsymbol{B}_h$ onto $\boldsymbol{E}_h$ without defining a horizontal coordinate system. However, when individual tensor elements, such as Z_{xy} or Z_{yx}, are considered, the definition of a coordinate system is required. Consequently, the coordinate representation of $\overline{Z}$ depends on the orientation of the coordinate system used.

Equation 1.19 represents the magnetotelluric transfer function orientated according to the coordinate system x, y. The magnetotelluric transfer function orientated in a x', y' coordinate system rotated clockwise through an angle α is then represented by

$$\overline{Z}'(\alpha) = \overline{R}(\alpha) \cdot \overline{Z}(\alpha) \cdot \overline{R}(-\alpha) \tag{1.24}$$

where $\overline{R}(\alpha)$ is the rotation matrix

$$\overline{R}(\alpha) = \begin{pmatrix} cos\alpha & sin\alpha \\ -sin\alpha & cos\alpha \end{pmatrix}. \tag{1.25}$$

Equation 1.24 can be written out explicitly for the individual components of the magnetotelluric transfer function, for example for the Z_{xy} or Z_{yx} components Equation 1.24 becomes

$$Z'_{xy}(\alpha) = Z_{xy}cos^2\alpha - \left(Z_{xx} - Z_{yy}\right) sin\alpha cos\alpha - Z_{yx}sin^2\alpha \tag{1.26}$$

$$Z'_{yx}(\alpha) = Z_{yx}cos^2\alpha - \left(Z_{xx} - Z_{yy}\right) sin\alpha cos\alpha - Z_{xy}sin^2\alpha. \tag{1.27}$$

As the magnetotelluric transfer function has a number of properties, or so-called *rotational invariants*, that hold for any orientation of the horizontal coordinate system. These rotational invariants can for example be used as dimensionality indicators or as a first guess for the resistivity structure of the subsurface. A simple example of such a rotational invariant can be deduced from Equation 1.26

$$Z'_{xy}(\alpha) - Z'_{yx}(\alpha) = Z_{xy} - Z_{yx} \tag{1.28}$$

which shows that the off-diagonal elements of $\overline{Z}$ are invariant under rotation.

Induction arrows

The vector representation of the ratios of the real and imaginary parts of the vertical to horizontal magnetic field components is called the induction arrow. Induction arrows are commonly used to assess if there are lateral variations in conductivity.

1.7 Distortion of the magnetotelluric signal

It is known that small near-surface conductive inhomogeneities and topography can cause distortion of the electromagnetic signal. Additionally large scale regional structures, like the coastline, a large mountain range in the vicinity of the survey area or the dominant strike direction of geological structures, can also cause distortion of the electromagnetic fields. All these distortions are commonly known as galvanic distortion.

1.7.1 Static shift

A well known example of galvanic distortion induced by amongst others near-surface inhomogeneities or topography, is the *static shift effect* [*Sternberg et al.*, 1988]. Its effect on the magnetotelluric data can be best described by a relative upward or downward shift in the amplitude of the apparent resistivity of the magnetotelluric transfer function from station to station, while the shape of the stations responses remains comparable (see Figure 1.14). As the static shift effect affects the resistivity model resulting from the measured magnetotelluric data, mitigation measures are necessary.

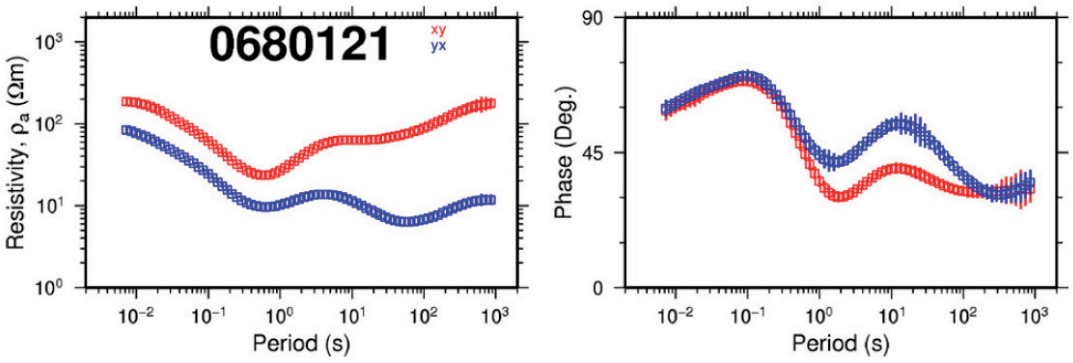

Figure 1.14: Static shift effect in a magnetotelluric sounding. Here recognized in the large separation of the XY and YX apparent resistivity curves at periods below 1 s. [*Árnason et al.*, 2010].

Several approaches are available to correct for the static shift effect. *Árnason et al.* [2010] for example, uses 1-D TEM[2] measurements to iteratively shift the invariant[3] of the magnetotelluric response towards the TEM response under the assumption that the TEM response reflects the true 1-D resistivity of the shallow subsurface. In other cases the magnetotelluric response is corrected by mapping the TEM apparent resistivity versus decay time response to the magnetotelluric apparent resistivity versus period response [*Sternberg et al.*, 1988]. Another approach is to correct for the static shift effect by smooth regularized joint inversion of the magnetotelluric data and static shifts. Ultimately, the last strategy to mitigate for the static shift effect is by incorporating the topography into the model mesh, under the condition of a sufficiently high resolution, and assuming that the 3-D inversion accommodates the correction.

Since several methods for static shift correction are available, it is often debated in geothermal industry which method is 'best'. It is worthwhile mentioning that although effective in many cases, not all available methods can be applied under all circumstances.

1.8 Dimensionality

Dimensionality distortions in the electromagnetic signal are caused by 2-D or 3-D structures in the subsurface and will be reflected in the chosen survey design and modelling strategy. Special care should be taken when the dimensionality of the

[2]Transient Electromagenetics (TEM) is a controlled-source electromagnetic method which measures a 1-D apparent resistivity versus decay time response of the shallow subsurface.

[3]Here the invariant of the magnetotelluric data is the average of the Z_{xy} and Z_{yx} components of the magnetotelluric transfer function. Generally computed by taking the geometric mean of the apparent resistivities ρ_{xy} and ρ_{yx} and the arithmetic mean of the phases of the two. The magnetotelluric response is assumed to be 2-D and rotated to its principal axis, e.g. $Z_{xx} = Z_{yy} = 0$.

structures in the subsurface is different from the dimensionality of the modelling code used. In those instances, inaccurate resistivity structures might be resolved by the modelling, leading to an erroneous geological interpretation of the inversion model. The dimensionality of a magnetotelluric data set can be assessed using tools such as induction arrows, rotational invariants, dimensionality indicators and Groom and Bailey distortion parameters.

A resistivity cross-section resulting from 1-D, 2-D and 3-D inversions of magnetotelluric data acquired in the Glass Mountain geothermal field in the USA is shown in Figure 1.15. In Figure 1.15 it can be observed that although the main resistivity structures are resolved by all three models, the differences between the models are significant. Differences in depth and shape of the conductive clay cap and the resistive geothermal reservoir are apparent. The elongated conductive structures in the 1-D resistivity cross-section are caused by the multi-dimensionality of the magnetotelluric data. See *Cumming and Mackie* [2010] for more details on the Glass Mountain case.

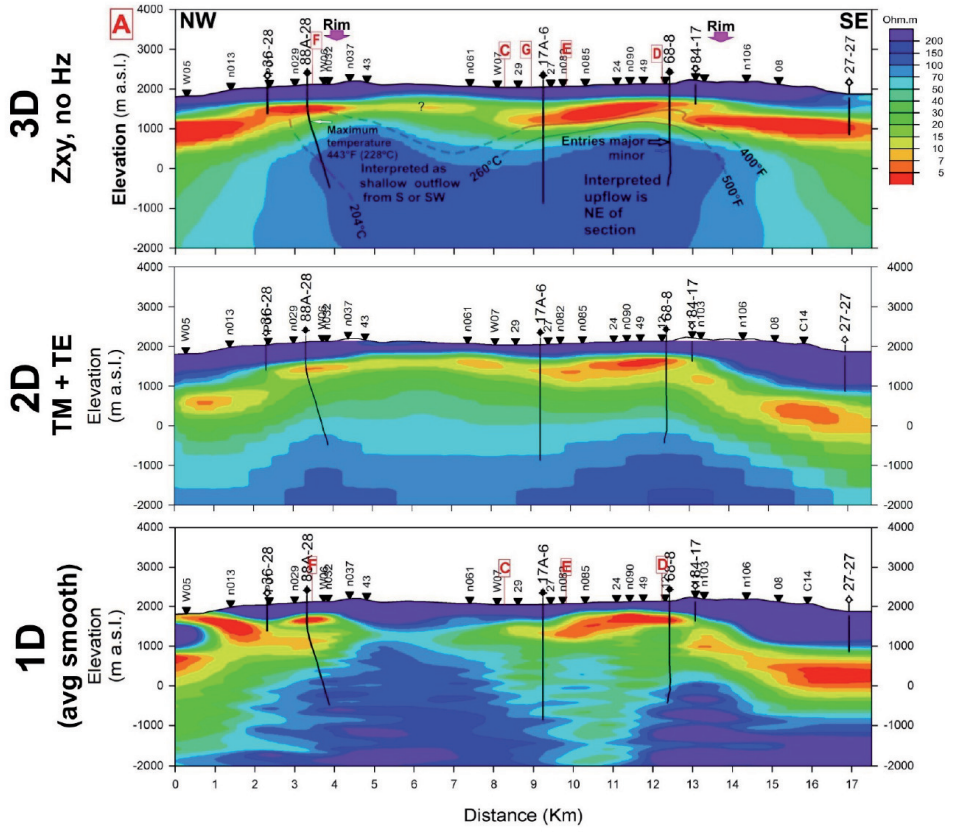

Figure 1.15: Cross-section with 1-D, 2-D and 3-D resitivity inversions of the magnetotelluric data from the Glass Mountain geothermal field. Wells, isotherms and magnetotelluric stations are given. Note the differences in shape and depth of the conductive clay cap and resistive geothermal reservoir between the inversion. For details see *Cumming and Mackie* [2010].

A regularly applied strategy in geothermal exploration to determine the reliability of a 2-D or 3-D inversion is a resistivity model of stitched 1-D (invariant) inversions. Independent of the dimensionality of the data, the main resistivity structures resolved by either 1-D, 2-D and 3-D inversions might be regarded as all credible. With respect to geothermal exploration *Cumming and Mackie* [2010] point out that for accurate well targeting a full assessment of at least 1-D and 2-D inversion models, but preferably 1-D and 3-D inversion models should be carried out. Care should be taken when utilizing this strategy, as the inverted component(s) of the magnetotelluric transfer function are likely to influence the result. See Section 1.6 Additionally, *van Leeuwen* [2016] suggests to run at least two 3-D inversion using differing inversion codes for accurate well targeting.

1.9 Cultural electromagnetic noise

A magnetotelluric sounding can also be distorted by man-made noise, often referred to as cultural electromagnetic noise. Cultural electromagnetic noise can be caused by, for example, power lines, subsurface pumps, anti-corrosion systems in buried pipelines, wind turbines, electric trains, electric fences, and mining areas. As the population and the electrification of the Earth are growing, the effects of cultural electromagnetic noise on magnetotelluric surveys will increase as well. There are already many areas where it is virtually impossible to carry out a magnetotelluric survey.

Cultural electromagnetic noise can be divided into *passive* and *active* electromagnetic noise. In addition to these to two types, a third type of cultural electromagnetic noise can be recognized, caused by, for example, passing vehicles or other artificial vibrations of the subsurface. This is often refereed to as motional noise. Logically, in densely populated areas the number of cultural electromagnetic noise sources will be greater than in quiet areas. It is also likely that in these densely populated areas the amplitudes of the noise will be larger, sometimes exceeding the amplitude of the natural electromagnetic signal. Examples of passive noise sources are, for example, roads, ditches, power lines, and pipelines, which distort the electromagnetic source field. Depending on the size of their local electromagnetic field, the influence on the measurements of passive noise sources can be avoided or minimized by placing the magnetotelluric stations a considerable distance away from these features.

Some of the features inducing passive electromagnetic noise can also serve as an active noise source when inducing an electromagnetic (secondary) field into the subsurface. To illustrate this, a power line serves as a primary source, potentially

generating passive noise, and the transmitted electrical power via this power line will generate active noise as it induces a secondary electromagnetic field. To put it more simply, all power consuming devices are potentially active noise sources. Examples of active noise sources are DC[4] railways, electric power transmission lines, subsurface pumping stations, and anti-corrosion systems in buried pipelines. Active noise will heavily disturb the measured electromagnetic spectra. When measuring far away enough from the noise source, its effect will be decreased, as illustrated in Figure 1.16.

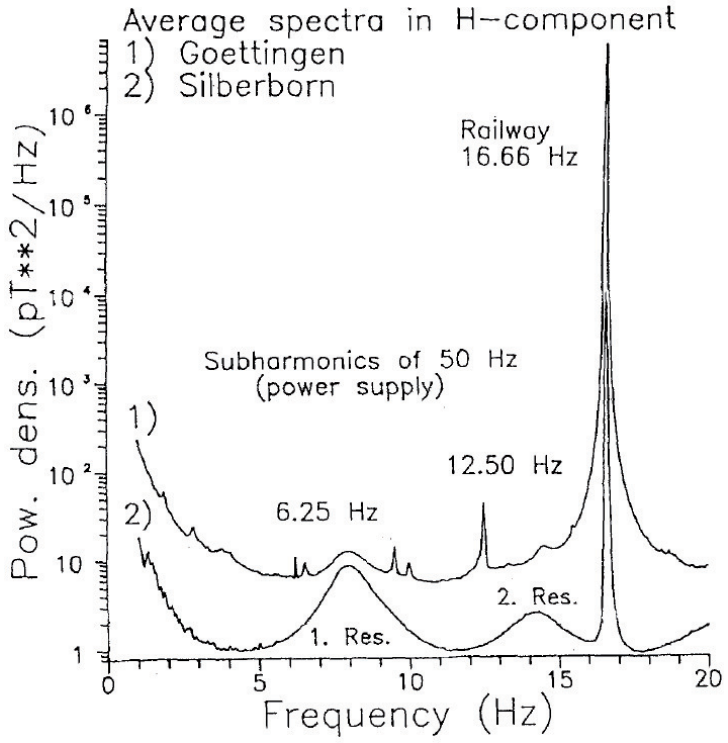

Figure 1.16: Electromagnetic noise spectra from two locations in Germany [*Junge*, 1996].

In Figure 1.16 the spectra of two locations 30 km apart are shown. At site 1, located close to an industrial region, the railway, the (sub)harmonics of the power lines, generating an electromagnetic signal at 50 Hz, and several minor peaks are easy to recognize and have a very large amplitude, while at site 2, which is far away from any industrial activity, only the railway is detected [*Junge*, 1996].

As it is not always possible to avoid all sources of cultural electromagnetic noise during a magnetotelluric field survey, cultural electromagnetic and other noise effects must be eliminated from the magnetotelluric data during data processing to obtain an accurate resistivity model of the subsurface during data processing.

[4]Direct Current

1.10 The magnetotelluric process in a birds eye view

In Figure 1.17 a flowchart of the entire process of a geothermal magnetotelluric survey from survey design to resistivity model interpretation is given. The various processes, actions and decisions are described in the following sections.

1.11 Data acquisition

Magnetotelluric surveys are conducted using data loggers measuring the five electromagnetic fields, B_x, B_y, B_z, E_x, and E_y. The electric field is measured using electrodes set up as two perpendicular dipoles, often orientated North-East and South-West. The electrodes are buried to account for day-night temperature variations in the upper few tens of centimetres of the subsurface and to keep the electrodes moist. A good conductivity between the electrodes and the surface is essential for a magnetotelluric sounding measuring good quality data. Magnetic coils measure the three components of the magnetic field. Two of these coils are positioned horizontally with a perpendicular orientation, measuring the horizontal magnetic fields, while a third coil is positioned vertically, measuring the vertical magnetic field. Since accurate and stable positioning of the coils is important, the coils are buried in shallow holes to prevent any external disturbances. As motional noise induced by wind can reduce the quality of the measured data, especially the cables connecting the electrodes should be protected by placing rocks or sand on the cables.

The general layout of a magnetotelluric station is shown in Figure 1.18. A GPS-receiver is connected to the data logger for time synchronization with the remote reference station. To power the data logger while measuring, a battery is also a part of the setup of a magnetotelluric station.

During a magnetotelluric survey, a remote station is often recording at an electromagnetically quiet location measuring simultaneously with the local magnetotelluric stations, see Section 1.12.2. Finding a good, quiet location for the remote reference station is always worth the effort for a successful magnetotelluric field campaign.

Depending on the depth of the target of the magnetotelluric survey and the local bulk electrical resistivity of the Earth, the magnetotelluric recording period varies from a few hours to several days, months or years. A possibility is to use Equation 1.4 (see Section 1.5) to estimate the desired magnetotelluric recording period for a survey.

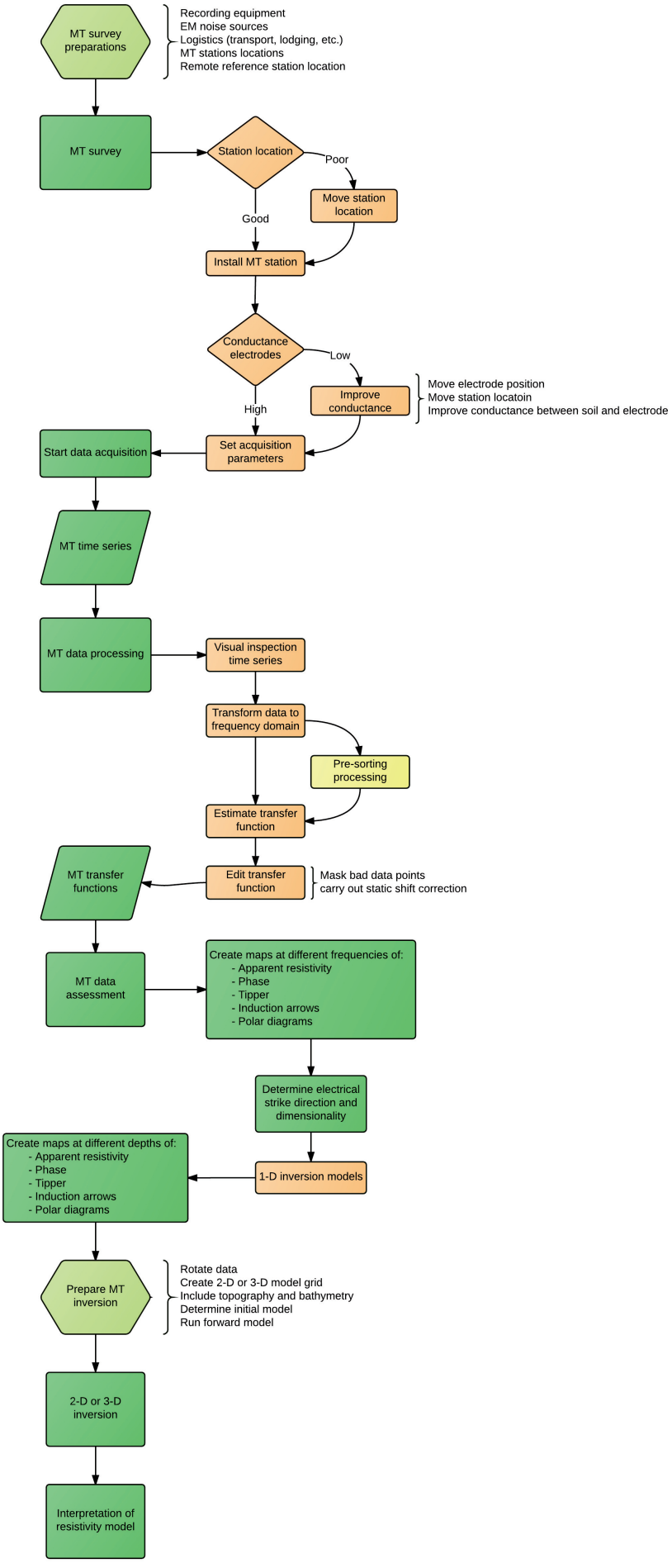

Figure 1.17: Flowchart of the magnetotelluric process.

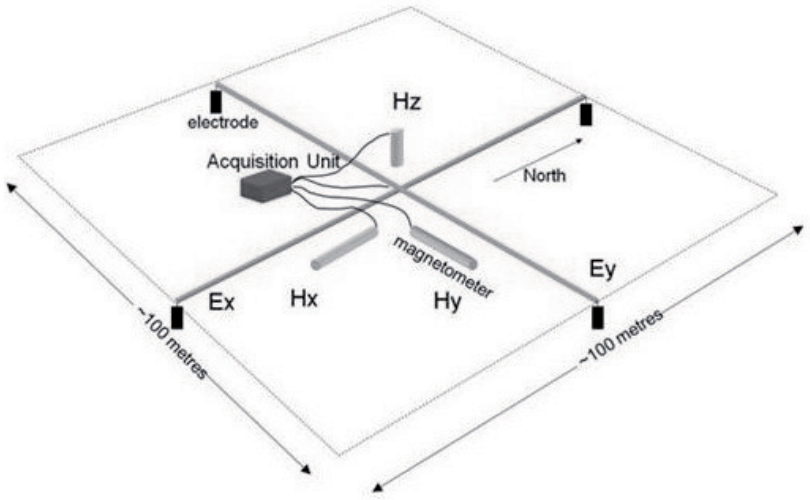

Figure 1.18: Generalize layout of a magnetotelluric station showing electric dipoles, magnetic coils, data logger, battery and GPS-receiver.

A more sophisticated strategy is to determine the desired period range of the survey and adjust to the magnetotelluric recording period accordingly. The period T can be determined using

$$T = \mu_0 \sigma \pi p^2 \tag{1.29}$$

which is a reformulation of the inverse of Equation 1.21 to compute the bulk apparent resistivity. To explore a geothermal reservoir from 0.5 to 5 km depth with an average bulk resistivity of 1 Ωm, a period T =1 to 100 s is necessary. In practice the resistivity of the surface is not homogeneous and this simple computation becomes more complex.

As a rule of thumb, the site occupation should be at least 100 times the largest period of interest. In this example a site occupation of at least 3 hours is necessary. For geothermal exploration purposes it is common to measure magnetotelluric data for roughly 18 to 24 hours. It is worthwhile to optimize the survey schedule to increase the magnetotelluric recording periods.

The survey grid layout is determined by the local topography, the size of the survey area, the available budget and time, and the expected dimensionality of the local geological structures. Ideally, station locations are pre-selected on the basis of maps, topography, geology, etc, using all available information and avoiding possible noise sources. However, before station deployment the magnetotelluric station locations should be re-assessed in the field and, if necessary, moved to another location. The site spacing of the profile or grid depends on the depth of the measured target. In geothermal exploration practice, several profile lines or a semi-regular grid layout with a site spacing of a half to two kilometres is the norm. When designing a survey

grid it frequently happens that a trade-off between budget and time is made. In those instances it is important to realize that the quality of the data measured prevails over the number of total stations occupied.

One factor influencing the magnetotelluric data quality is the accuracy of the station layout in the field. The easiest way to acquire good data is to work accurately and ensure that the field crew is working precisely. Too often sites are set up too close to possible (cultural) electromagnetic noise sources and with an inaccurate positioning of the coils or electrodes. Another straightforward mitigation procedure for distortion of the electrical field is ensuring good conductance between the electrodes and the Earth. Thinking about strategies to tackle the possible difficulties of the terrain in the survey area and scouting the station locations prior to the field work or station occupation often increases the average data quality of the magnetotelluric survey.

Finally, the strength of the magnetic field is influenced by the space weather (see also Section 1.5, for the magnetic field this is forecasted and reported online as the Kp-index. The higher the Kp-index at a location, the stronger the local magnetic field strength, and the more likely the acquired magnetotelluric data is of good quality. Consequently, if possible, a magnetotelluric survey should be carried out during a period of forecasted high Kp-indeces. The altitude at which the magnetotelluric survey is conducted also influences the magnetic field strength. At high altitudes, the magnetic field strength is generally weaker. This should be accounted for by adjusting the recording settings of the data logger in the field.

1.11.1 Quality check of recorded magnetotelluric data

Recorded magnetotelluric data can be quality checked using a variety of observations and tools:

1. The number of saturated records in the recorded data should be low. A high number of saturated records means that the (amplified) recorded signal exceeds the scale range of the analogue-to-digital converter of the magnetotelluric data logger and is cut-off.
2. Visual inspection of the recorded magnetotelluric raw time series. The more noisy the raw time series data look, the lower the quality of the station response is likely to be. Obvious spikes and noisy events are easily observed in time series plots, as is drift in one of the channels. As the raw time series of higher sampling rates generally look more noisy, it becomes more difficult to detect noise in those raw time series. This is illustrated in Figures 1.19 and 1.20 for a high and a low sampling rate.

In Figure 1.19 10 minutes of raw times series of a the horizontal electromagnetic fields of a magnetotelluric station are shown.

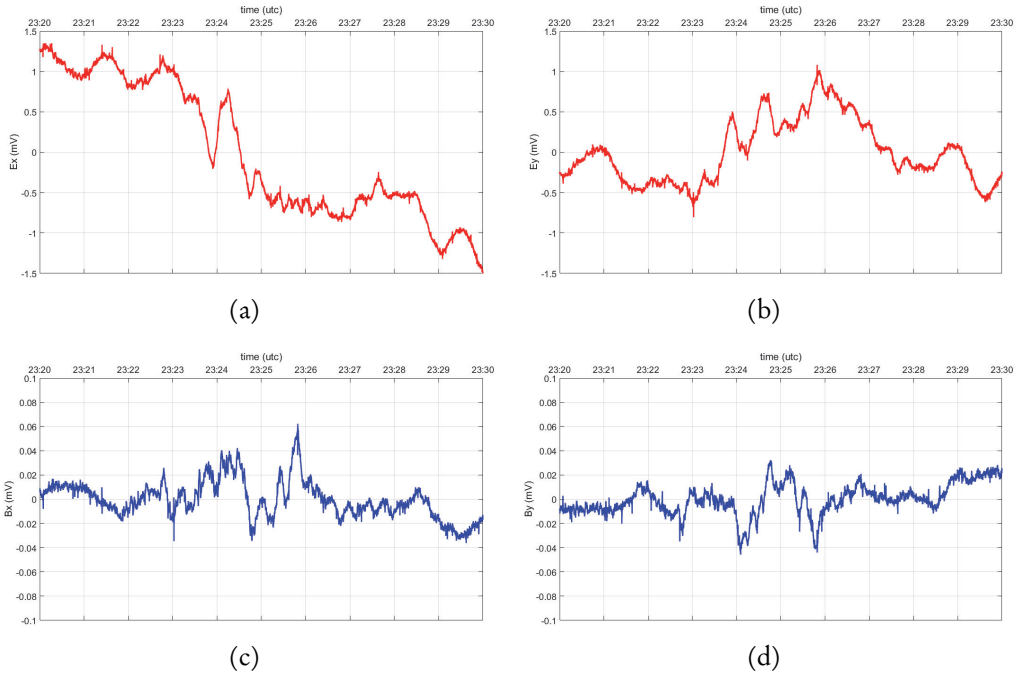

Figure 1.19: Raw time series of the horizontal electromagnetic fields as recorded at a magnetotelluric station at a sampling rate of 15 Hz. The displayed time spans 10 minutes (9,000 measurements). The raw time series data of the horizontal electric fields (red) show a good signal with some high frequency noise ((a) and (b)). The raw time series data of the electric E_x field as shown in Figure (a) shows some drift. This is probably the result of a variable contact resistance between the electrodes and the subsurface. The raw time series data of the horizontal magnetic fields (blue) show good quality magnetic signal with some overprints of some far away lighting effects ((c) and (d)).

3. Spectra of the recorded fields can also be utilized to assess the recorded data quality. A spectrum with narrow (noise) peaks (and harmonics) is more likely to produce a good magnetotelluric response in comparison to a field with a spectrum showing wide peaks. In Figure 1.21 the power spectrum of the 2,400 Hz sampled magnetotelluric data (as shown in Figure 1.20) is shown. In this Figure, several sharp spikes are visible. Where the 50 Hz spike is related to electric power lines, the other spikes appearing at 100 Hz, 150 Hz, 200 Hz, etc., are all harmonics of this signal.

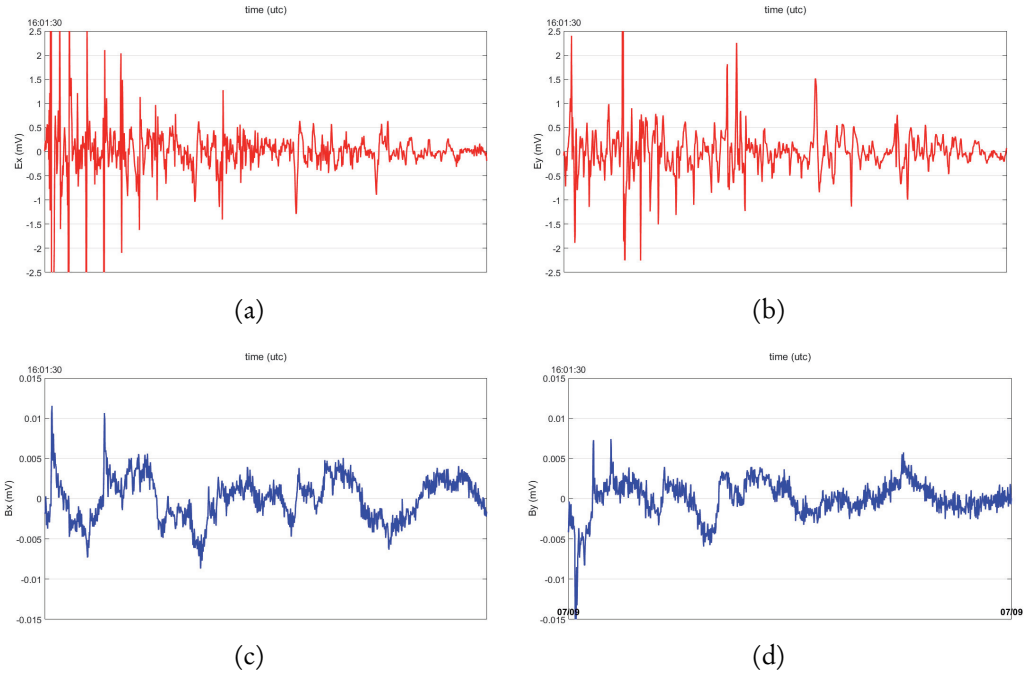

Figure 1.20: Raw time series of the horizontal electromagnetic fields as recorded at a magnetotelluric station at a sampling rate of 2,400 Hz. The displayed time spans 0.5 seconds (1,200 measurements). In the recorded electric field raw time series data (red) spikes overprinting the signal can be observed at early times ((a) and (b)). The raw time series data of the magnetic fields of this recording (blue) have some spikes at similar times as in the electric field raw times series data ((c) and (d)).

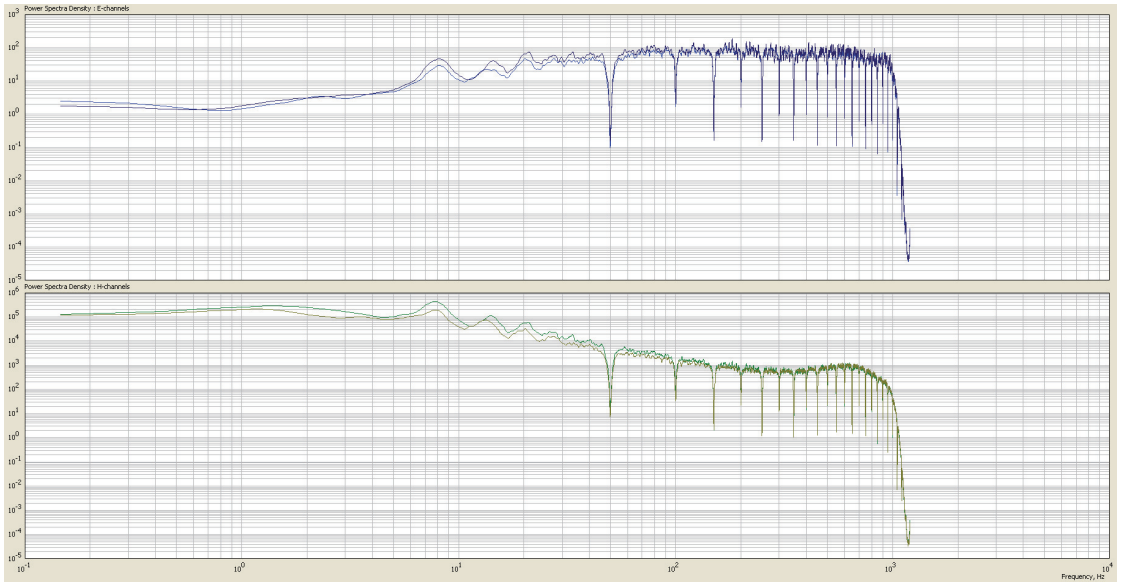

Figure 1.21: Power spectrum of the magnetotelluric data of the time series as shown in Figure 1.20 for the electric and the horizontal magnetic fields. The negative spikes in this power spectrum are in fact the result of a notch filter, removing the (sub)harmonics of the the 50 Hz power line signal during acquisition.

4. A spectrogram is a visual representation of the spectrum of a set of frequencies in "time". Noisy events are characterized by high amplitudes within the spectrogram, while a clean magnetotelluric data set is indicated by a relatively low amplitude, homogeneous spectrogram. In Figure 1.22 spectrograms of recorded horizontal electromagnetic fields of the same magnetotelluric data as shown in Figures 1.20 and 1.21 are plotted.

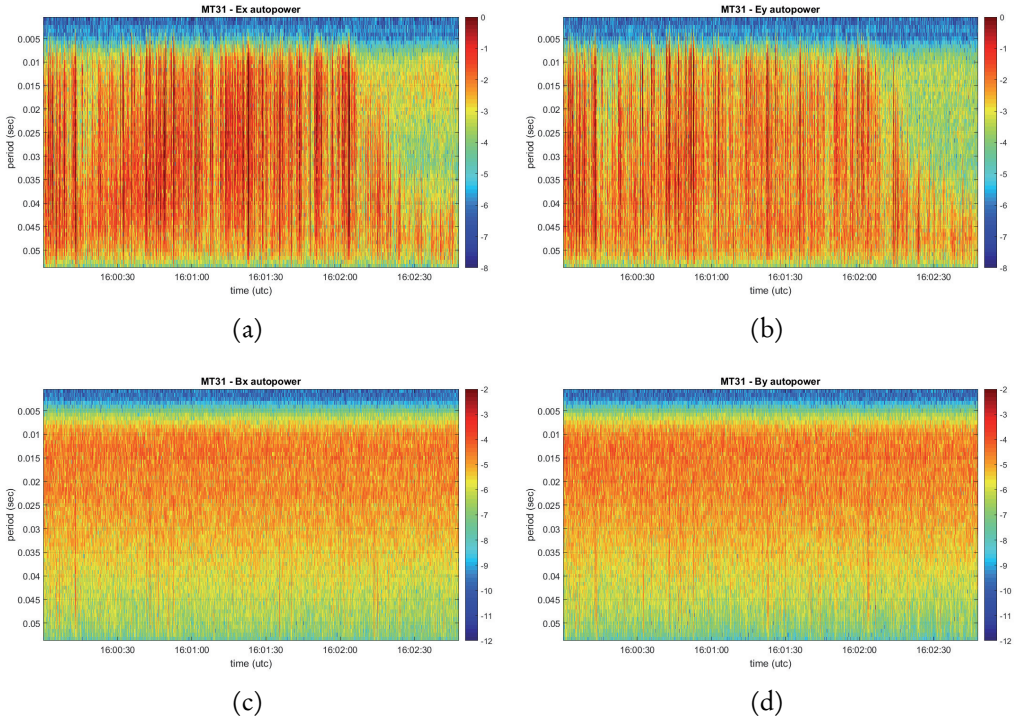

Figure 1.22: Spectrograms of the 2,400 Hz recorded magnetotelluric data of Figure 1.20. The frequency range spanned by these spectrograms is 20 (0.05 s) to 200 Hz (0.005 s). Within this frequency range some vertical spikes are visible in the magnetic fields ((c) and (d)), while the high amplitudes around 0.02 s (50 Hz) are contributed to by power lines. In the spectorgram of the electric fields as given in Figures (a) and (b) a large number of high amplitude spikes can be observed. These spikes are probably related to lightning strikes.

5. Many magnetotelluric software packages offer the possibility to estimate automatically the magnetotelluric transfer function and magnetotelluric station response without further processing. A look at the station response produced using this functionality provides a relatively good estimation of the quality of the measured magnetotelluric data. However, this "preliminary" response should be treated with caution as experience shows that unwanted processing effects are often present in these estimations and manual editing is necessary.

1.12 Estimation of the magnetotelluric transfer function

To recover the conductivity structure of the subsurface in the spectral domain, the magnetotelluric transfer function $\overline{Z}$ has to be estimated from Equations 1.12 or 1.19. In the case of actual magnetotelluric measurements, $\boldsymbol{E}$ and $\boldsymbol{B}$ contain noise and therefore not only $\overline{Z}$ but also its uncertainty $\delta\overline{Z}$ has to be estimated. Similarly, the uncertainty for the vertical magnetic transfer function should be estimated.

1.12.1 Data processing theory

The magnetotelluric transfer function (Equation 1.12) and the vertical magnetic transfer function (Equation 1.13) can in the spectral domain be generalized using the expression:

$$X = Z_1 \cdot Y_1 + Z_2 \cdot Y_2 \tag{1.30}$$

where X is the predicted channel associated with either E_x, E_y or B_z and Y_1 and Y_2 being the predicting channels B_x and B_y. Z_1 and Z_2 are the magnetotelluric transfer functions of a linear system of equations, e.g. Z_{xx} and Z_{xy} associated with E_x, B_x, and B_y. The magnetotelluric transfer function can be estimated following:

$$\overline{Z} = (\boldsymbol{E} \otimes \boldsymbol{B}^*) \cdot (\boldsymbol{B} \otimes \boldsymbol{B}^*)^{-1} \tag{1.31}$$

where $\otimes$ is the outer product and * denotes the complex conjugate.

At this point it is necessary to mention that in magnetotelluric data processing the raw time-dependent magnetotelluric data is transformed to the frequency domain. To fully utilize all measured frequencies, the time-series are decimated[5], creating a number of time-dependent magnetotelluric data sets with decreasing sampling rates. Depending on the sampling rate and the number of samples present, each decimation level spans a number of frequencies. Thereafter, the individual samples are stacked along pre-defined overlapping time-windows. The magnetotelluric data are smoothed by applying, for example, a running average filter to the stacked time windows. Finally, the stacked time-windows are transformed to the frequency domain using a direct or fast Fourier transform. Consequently the auto- and cross-spectra in Equation 1.31 comprise a number of stacked and smoothed Fourier coefficients of the magnetotelluric data. It is important to realize that the decimation scheme, window length, type of smoothing filter are all choices affecting the final processing result.

[5]The process of reducing the sampling rate of the measured signal is called *decimation*.

In the case where cultural electromagnetic noise is included in the measurements, Equation 1.30 becomes:

$$Z = \frac{(\boldsymbol{Y}_0 + \boldsymbol{n}_Y)}{(\boldsymbol{X}_0 + \boldsymbol{n}_X)} \tag{1.32}$$

where $\boldsymbol{X}_0$ and $\boldsymbol{Y}_0$ are the predicted respectively predicting channels without noise, and $\boldsymbol{n}_X$ and $\boldsymbol{n}_Y$ are the recorded noise in these channels.

As solving the system of equations of Equation 1.31 using the least-squares principle delivers unreliable results when applied to real magnetotelluric data, it is hardly used in practice. Robust processing approaches, such as *Egbert and Booker* [1986]; *Chave and Thomson* [1989, 2004]; *Larsen et al.* [1996] are used instead to estimate the magnetotelluric transfer function. These approaches utilize unbiased statistical estimators and data-adaptive weighting-schemes for the calculation of the magnetotelluric transfer function. In robust processing approaches the norm of the measured errors ε in $X = (Z_1 \cdot Y_1 + Z_2 \cdot Y_2) + \varepsilon$ is minimized without letting extreme outliers dominate the result. A generalization of the robust processing approache is described in the following:

1. The least-squares estimate of the magnetotelluric transfer function is computed.
2. The residual r and the residual sum of squares are calculated for each channel: $r = X - (Z_1 \cdot Y_1 + Z_2 \cdot Y_2)$. Here, Z_1 and Z_1 are the least-squares estimates of the magnetotelluric transfer function. At this point a scale factor to make r independent of size of the input data, is calculated as well.
3. The weights and the chosen estimate, e.g. M-estimate [*Chave and Thomson*, 1989] or bounded influence estimate [*Chave and Thomson*, 2004], are computed.
4. Steps 1 to 3 are repeated until the change in the residual sum of squares is below 1%
5. The data points with zero weight are eliminated from the data.
6. Again, steps 1 to 3 are repeated until the change in the residual sum of squares is below 1%, but this time with a fixed scale factor.
7. The data fit of this final estimate of the magnetotelluric transfer function to the measured magnetotelluric data is evaluated and the confidence bands are calculated.

1.12.2 Remote reference processing

To optimize the estimated magnetotelluric transfer function several additional processing methods are available which can be applied additionally to or instead of the robust processing approaches. Most important and used in almost every magnetotelluric survey is the remote reference method [*Gamble et al.*, 1979]. The remote ref-

erence method utilizes the plane wave assumption by simultaneously measuring the horizontal magnetic field ($\boldsymbol{B}_R$) at a remote station. Assuming uncorrelated magnetic noise between the local and the remote magnetotelluric station, the noise in the local station can be eliminated by substituting the remotely recorded magnetic field into Equation 1.31.

$$\overline{Z} = (\boldsymbol{E} \otimes \boldsymbol{B}_R^*) \cdot (\boldsymbol{B} \otimes \boldsymbol{B}_R^*)^{-1} . \tag{1.33}$$

Assuming uncorrelated magnetic noise between the recorded local and the remote station, the noise in the local station is eliminated according to $\boldsymbol{n}_B \cdot \boldsymbol{n}_{B_R} = 0$, and the noise term will disappear in Equation 1.33.

In Figure 1.23 the effect of the remote reference method is illustrated by two plots of a single magnetotelluric station. In the left plot, the station is processed without remotely recorded magnetic fields, while in the plot to the right, the remotely recorded magnetic fields are used. The result is clear, the downward bias present in the apparent resistivity of the local processing results between 10 and 0.1 Hz is removed in the remote reference processing results.

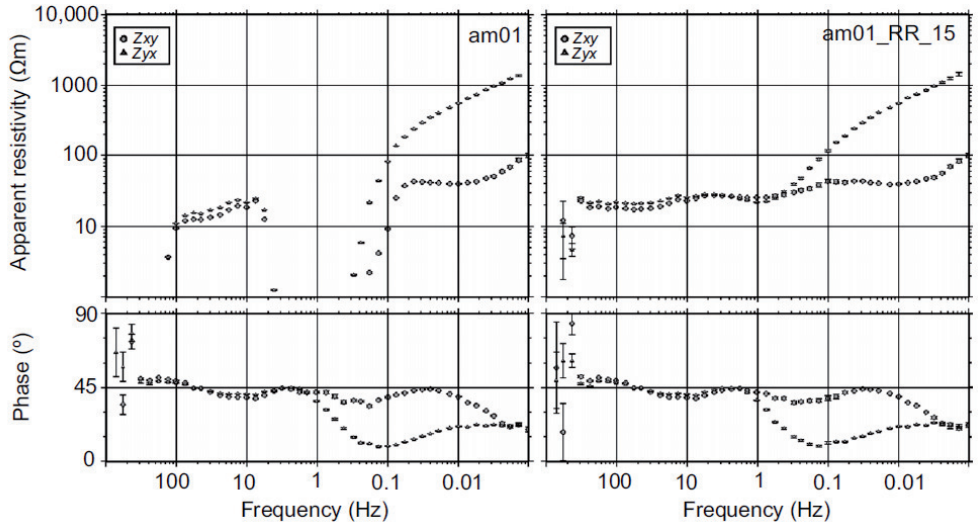

Figure 1.23: magnetotelluric data recorded on Amchitka Island, Alaska. Left processed without remote reference, right processing with with remote reference. See *Unsworth et al.* [2007].

1.12.3 Coherence sorting

Incorporated into most commercial processing software packages, to distinguish signal from noise, is coherence-sorting. Coherence-sorting is an easy to implement approach that evaluates the coherence between input and output channels and is applied before the estimation of the magnetotelluric transfer function.

In Figure 1.24 the bivariate coherence of the horizontal electric with the horizontal magnetic fields is plotted. The data shown here is from the same magnetotelluric station as discussed earlier in Section 1.11.1. An electric field is linearly related with the horizontal magnetic fields through Equation 1.30. Consequently, high coherences indicate good quality data, while poor quality data have a low coherence. During processing one can, for example, decide to remove all samples with a coherence below 0.9 from the magnetotelluric data set. Although practical, this method is not always effective.

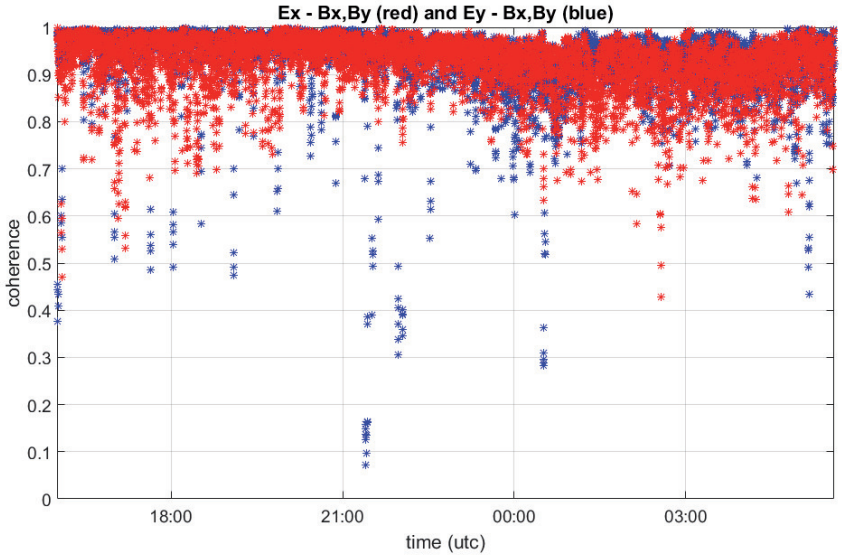

Figure 1.24: Bivariate coherence of channels E_x (red) and E_y (blue) with channels B_x and B_y. High coherences indicate good data, while low coherences indicate bad data.

1.13 Inversion and modelling

To estimate the subsurface resistivity distribution in the Earth's subsurface, the observed magnetotelluric data needs to be inverted. The process of inversion is iterative and is aimed at finding one or more resistivity models whose predicted responses matches the observed data as good as possible. Depending on the properties of the magnetotelluric response and the dimensionality of the local geology, the inversion can be done in 1-D, 2-D or 3-D. As the resulting inversion model is non-unique, i.e., several resistivity models fit the observed magnetotelluric data equally well. Consequently, the inversion of magnetotelluric data is inherently unstable, or ill-posed, and the solution estimated must be constrained using other sources of information.

Although an extensive discourse on inversion theory is beyond the scope of this course, a condensed formulation of the inverse problem will be given.

The inverse problem

The inverse problem can be formulated as:

$$\boldsymbol{d} = F\boldsymbol{m} + \boldsymbol{e} \tag{1.34}$$

where $\boldsymbol{d}$ is the data space, a vector containing the observed data, e.g., the magnetotelluric transfer function, the apparent resistivity and phase. The vector $\boldsymbol{e}$ contains the data errors of $\boldsymbol{d}$. The model space $\boldsymbol{m}$ represents the real resistivity values of the Earth, while F is a forward function predicting the theoretical values of the data for a hypothetical (model) representation of the Earth. In the theoretical case that $\boldsymbol{e} = 0$, the solution to Equation 1.34 becomes $\boldsymbol{m} = F^{-1}(\boldsymbol{d})$, hence the term inverse problem. As finding F^{-1} is not considered realistic, the challenge becomes to find the best estimate of $\boldsymbol{m}$:

$$\tilde{\boldsymbol{m}} = G(\boldsymbol{d}) \tag{1.35}$$

where G is a meaningful substitute of F^{-1}.

Although in electromagnetics the solution to the inverse problem is not linear, it is illustrative to discuss it here. For finite-dimensional model spaces, the forward function is a linear transformation and can be expressed as:

$$F(\boldsymbol{m}) = \boldsymbol{A}\boldsymbol{m} \tag{1.36}$$

where $\boldsymbol{A}$ is a $N \times M$ matrix with the vectors of the function a_i^T as its rows. The linear operations carried out by F are defined by the right-hand side of 1.36

An approach to solve the nonlinear inverse problem is to linearize it. This is done by expanding Equation 1.36 around a reference model $\boldsymbol{m}_*$. A first-order approximation of the functional will then be

$$\bar{F}(\boldsymbol{m}) = F(\boldsymbol{m}_*) + \boldsymbol{A}_{\boldsymbol{m}_*}(m - m_*)\,. \tag{1.37}$$

In Equation 1.37, $\boldsymbol{A}$ is the Fréchet derivative of F, where F is a linear transformation. In geophysical inversion theory it contains the partial derivatives of the forward functions F_i and is referred to as the *Jacobian* matrix.

The basis for much geophysical inverse theory is the least-squares estimation. A least-squared solution is defined as finding the minimum solution of a fitting function, estimating the goodness of the fit between the model and the observed data. This data

misfit can be expressed by a *penalty* function

$$\Phi(\boldsymbol{m}) = (\boldsymbol{d} - F(\boldsymbol{m}))^T \overline{\boldsymbol{W}} (\boldsymbol{d} - F(\boldsymbol{m})) \tag{1.38}$$

where $\overline{\boldsymbol{W}}$ is the weight matrix containing pre-assigned weights, or the data covariance matrix, and $\boldsymbol{r} = \boldsymbol{d} - F(\boldsymbol{m})$ is the residual vector. Minimizing $\Phi(\boldsymbol{m})$ is done by starting from some initial model and iteratively solving the inverse problem until a certain data misfit is reached.

The above holds for problems which are mixed-determined, meaning that parts of the solution are constrained by the observed data, while others are not. In practice most electromagnetic inversion problems are under-determined, the number of unknown parameters is larger than the number of observations $N > M$. An approach to define a well-posed problem[6] is the damped least-squares estimate.

$$\Omega(\boldsymbol{m}) \leq \mu \tag{1.39}$$

in which $\mu \neq 0$ and Ω is the positive-valued *stabilizing functional*. This functional is designed to penalize undesired properties of $\boldsymbol{m}$. *Regularization* of the solution of the inverse problem comprises finding the minimum solution of $\Omega(\boldsymbol{m})$ subject to Equation 1.39

$$\Psi(\boldsymbol{m}) = \Phi(\boldsymbol{m}) + \lambda\Omega(\boldsymbol{m}) \tag{1.40}$$

where $\lambda > 0$ is the *regularization parameter* which is determined by μ.

Finally, the stabilizing functional, which is a measure of the spatial roughness of a model, is defined as

$$\Omega(\boldsymbol{m}) = (m - m_0)^T \overline{\boldsymbol{K}} (m - m_0) \tag{1.41}$$

where $\boldsymbol{m}_0$ is an initial or starting model and $\overline{\boldsymbol{K}}$ is a positive semi-definite matrix, also referred to as the model covariance matrix. The structure of penalty can be interpreted as an inverse a priori model covariance matrix.

By substituting Equations 1.38 and 1.41 into Equation 1.40, the damped least-squares functional becomes

$$\Psi(\boldsymbol{m}) = (\boldsymbol{d} - F(\boldsymbol{m}))^T \overline{\boldsymbol{W}} (\boldsymbol{d} - F(\boldsymbol{m})) + \lambda (m - m_0)^T \overline{\boldsymbol{K}} (m - m_0)\,. \tag{1.42}$$

By utilizing different approaches and techniques, the majority of the electromagnetic inversion algorithms try to minimize the damped least-squares functional

[6] A well-posed problem is one where the solution to the problem 1) exists, 2) is unique, and 3) is stable [*Hadamard*, 1902]

of Equation 1.42 efficiently.

1.14 Geothermal interpretation of resistivity models

When it comes to geological interpretation, the geothermal play type of the geothermal system explored should be considered first. Depending on the dominating factor determining the subsurface electrical resistivity, a geological interpretation can be made. When, for example, there is a limited volcanic component in a sedimentary geothermal system, clay alteration mineralogy will probably not be the main contributor to the resistivity of the subsurface. In such cases, it can for example be expected that the porosity and permeability or fluid composition form a significant factor in the resistivity of the subsurface for this geothermal project.

A scenario as described above is applicable for a geothermal project in Western Turkey of which a resistivity cross section including the geological interpretation is shown in Figure 1.25. Here, a recent exploration well drilled into the inferred geothermal reservoir delivered information improving the interpretation of the inversion model. The high conductivity is caused by weathered volcanic pyroclastics. The moderate resistivity structure below is related to an ophiolite complex, while the basement consists of equally resistive marble and limestones and was penetrated by the exploration well at a depth of approximately 2,500 m bsl. Having good porosity, this formation forms the geothermal reservoir with a temperature of 120 °C. For this geothermal project it can, for example, be anticipated that the lithology (rock composition) and/or porosity and permeability form a significant factor in the resistivity of the subsurface.

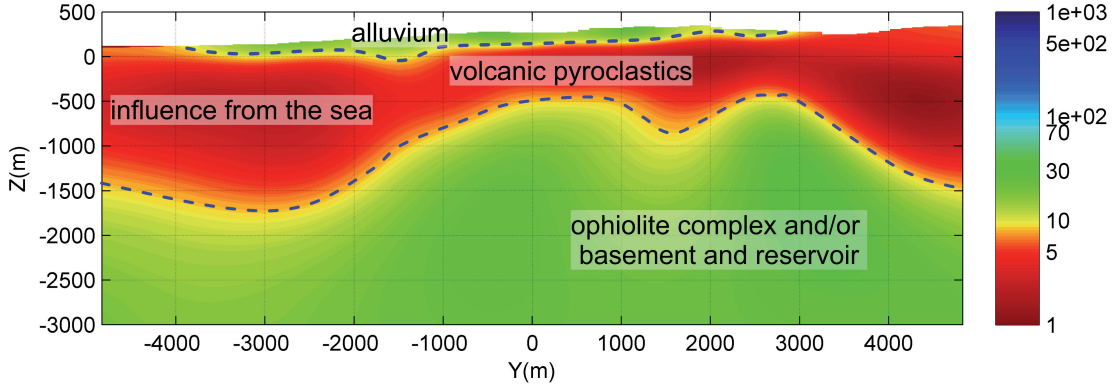

Figure 1.25: Resistivity cross section of a geothermal prospect in Turkey. The inferred geological formations or other factors corresponding to the resistivity structures are shown. The interpreted layering is highlighted by blue dotted lines.

Another interpretation scenario can be found in the Philippines (see Figure 1.26). In this geothermal project, a resistivity model is encountered that is challenging to interpret. Since the volcanic activity which formed the local geology is fossil, it has been decided to categorize this geothermal system as a plutonic geothermal play type. The resistivity structures imaged by the inversion, as well as the expected temperatures in the subsurface, indicate that the resistivity structure of the subsurface is largely controlled by hydrothermal alteration mineralogy. Geological field work indicated the presence of clay alteration minerals in a composition related to a temperature regime of 200 to 250 °C, a strong indication that the very low resistivity in the shallow subsurface is probably related to high temperature volcanic activity. As temperatures at these depths are currently significantly lower and volcanic activity is no longer present, it is likely that the high temperatures related to the observed conductive hydrothermal alteration mineralogy are also not present. In this case it can be concluded that the observed resistivity structure is a remnant temperature imprint of a cooling volcanic system. Since the resistivity structure below the shallow conductive layer is characterized by lateral resistivity variations, it can be assumed that the current temperature and porosity and permeability distribution is not laterally homogeneous within this layer. A theory might be that the areas with decreased resistivity values are related to increased porosity and permeability. Or, in other words, fracture driven fluid flow, providing the geothermal system with its hot fluids. The location and orientation of these zones coincides with the inferred faults in the survey area.

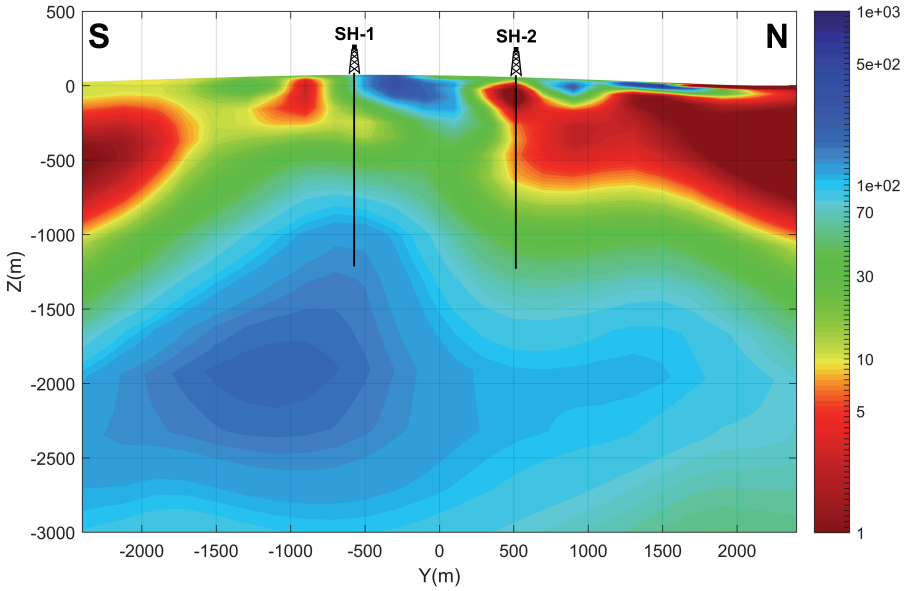

Figure 1.26: Resistivity cross section of a geothermal prospect in the Philippines. Two exploration wells are shown as well. The conductivities in the model correspond to clay alteration minerals formed at a higher temperature then the current rock temperature. Resistive anomalies coincide with faulted areas.

The two examples above illustrate that care should be taken when geologically interpreting a resistivity inversion model. Inferring an upflow clay-cap scenario is in general too simplistic and interpretation towards such a model can be costly. All additional geological and geochemical information should be used in the interpretation of the inversion resistivity model as well. To distinguish robust resistivity structures from model artefacts it is suggested to use at least a 1-D and a 3-D resistivity model of the geothermal system for interpretation purposes (see Section 1.8). When the locations of exploration wells have to be determined, it is recommended to use 3-D resistivity models generated by two different inversion codes.

This last point is illustrated by Figure 1.27 in which the resistivity maps at a constant elevation of -1,000 m of two 3-D resistivity models of the same magnetotelluric data set, but inverted by two different inversion codes, are shown. While the main resistivity structures of the model appear to be similar, the differences between the two models are also apparent. As the goodness of fit between the model and the observed data can be equally good for different inversion solutions, both models are an equally valid representation of the observed data. When interpreting inversion models and positioning wells on the basis of these models, this should be taken into account.

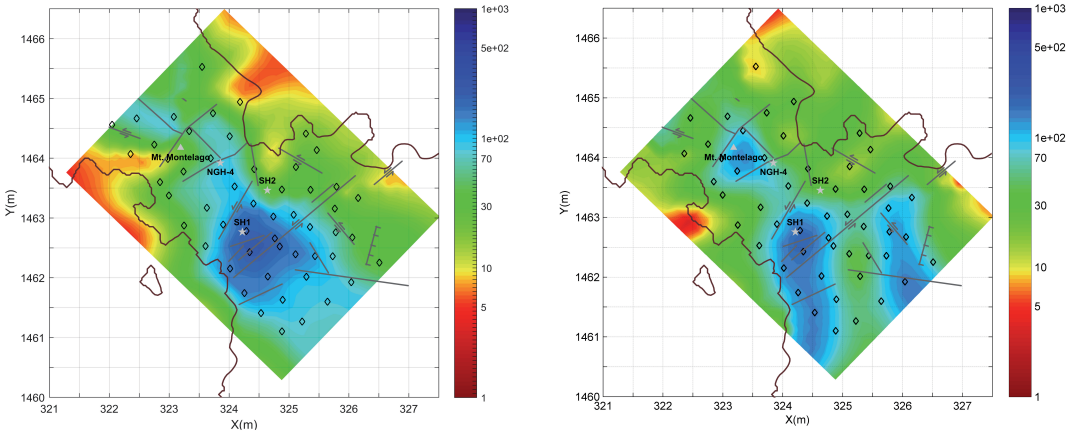

(a) (b)

Figure 1.27: Two inversion results of different inversion codes applied to the same magnetotelluric data set. Shown are resistivity maps at a depth of 1,000 m b.s.l. Indicated are faults and the main volcano in the area. Coast lines and main roads are shown as well. Resistivity values in Ω.m. (a) Inversion result using ModEM [*Egbert and Kelbert*, 2012] and (b) inversion result using WSINV3DMT [*Siripunvaraporn et al.*, 2005].

Bibliography

Arango, C., A. Marcuello, J. Ledo, and P. Queralt (2009), 3d magnetotelluric characterization of the geothermal anomaly in the llucmajor aquifer system (majorca, spain), *Journal of Applied Geophysics*, *68*, 479–488.

Archie, G. (1942), The electrical resistivity log as an aid in determining some reservoir characteristics, *Trans. AIME 146*, p. 54–67.

Árnason, K., H. Eysteinsson, and G. Páll Hersir (2010), Joint 1d inversion of tem and mt data and 3d inversion of mt data in the hengill area, sw iceland, *Geothermics*, *39*, 13–34.

Axelsson, G. (2013), Conceptual models of geothermal systems - introduction, Short Course V on Conceptual Modelling of Geothermal Systems, organized by UNU-GTP and LaGeo, in Santa Tecla, El Salvador.

Bibby, H., T. Caldwell, F. Davey, and T. Webb (1995), Geophysical evidence on the structure of the taupo volcanic zone and its hydrothermal circulation, *Journal of Volcanology and Geothermal Researc*, *68*, 29–58.

Bujakowski, W., A. Barbacki, B. Czerwińska, L. Pająk, M. Pussak, M. Stefaniuk, and Z. Trzeńiowski (2010), Integrated seismic and magnetotelluric exploration of the skierniewice, poland, geothermal test site, *Geothermics*, *39*, 78–93.

Cagniard, L. (1953), Basic theory of the magnetotelluric method of geophysical prospecting, *Geophysics*, *18*, 605–635.

Chave, A., and D. Thomson (1989), Sine comments on magnetotelluric response function estimation, *Journal of Geophysical Research*, *94*, 14 215–14 225.

Chave, A., and D. Thomson (2004), Bounded influence estimation of magnetotelluric response functions, *Geophysics Journal International*, *157*, 988–1006.

Cumming, W., and R. Mackie (2010), Resistivity imaging of geothermal resources using 1d,2d and 3d mt inversion and tdem static shift correction illustrated by a glass mountain case history, in *Proceedings World Geothermal Congress 2010*, Bali, Indonesia.

Dickson, M., and M. Fanelli (2004), What is geothermal energy?, online.

Didana, Y., S. Thiel, and H. Graham (2015), Magnetotelluric characterization of the habanero geothermal egs project: Initial results on fluid injection monitoring, in *Proceedings World Geothermal Congress 2015*, Melbourne, Australia.

Egbert, G., and J. Booker (1986), Robust estimation of geomagnetic transfer functions, *Geophysical Journal of the Royal Astronomical Society*, *87*, 173–194.

Egbert, G., and A. Kelbert (2012), Computational recipes for electromagnetic inverse problems, *Geophysical Journal International*, *189*, 251–267.

Flóvenz, O., E. Spangenberg, J. Kulenkampff, K. Árnason, R. Karlsdóttir, and E. Huenges (2005), The role of electrical interface conduction in geothermal exploration, in *Proceedings World Geothermal Congress 2005*, Antalya, Turkey.

Gamble, T., W. Goubau, and J. Clarke (1979), Magnetotellurics with a remote reference, *Geophysics*, *44*, 53–68.

Geiermann, J., and E. Schill (2010), 2-d magnetotellurics at the geothermal site at soultz-sous-forêts: Resistivity distribution to about 3000m depth, *Comptes Rendus Geoscience*, *342*, 587–599.

Grant, M., and P. Bixley (1982), *Geothermal Reservoir Engineering - Second Edition*, Academic Press.

Hadamard, J. (1902), Sur les problèmes aux dérivés partielles et leur signification physique, *Princeton University Bulletin*, pp. 49–52.

Heise, W., G. Caldwell, B. H.M., and B. S.C. (2008), Three-dimensional modelling of magnetotelluric data from the rotokawa geothermal field, taupo volcanic zone, new zealand, *Geophysical Journal International*, *173*, 740–750.

Hersir, G., K. Árnason, and A. Vilhjálmsson (2013), 3d inversion of magnetotelluric (mt) resistivity data from krýsuvík high temperature geothermal area in sw iceland, in *PROCEEDINGS, Thirty-Eighth Workshop on Geothermal Reservoir Engineering*, Stanford University, Stanford, California.

Junge, A. (1996), Characerization of and correction for cultural noise, *Surveys in Geophysics*, *17*, 361–391.

Larsen, J., R. Mackie, A. Manzella, A. Fiordelisi, and S. Rieven (1996), Robust smooth magnetotelluric transfer functions, *Geophysical Journal International*, *124*, 801–819.

Manzella, A., V. Spichak, P. Pushkarev, D. Sileva, B. Oskooi, G. Ruggieri, and Y. Sizov (2006), Deep fluid circulation in the travale geothermal area and its relation with tectonic structure investigated by a magnetotelluric survey, *Proceedings, 31st Workshop on Geothermal Reservoir Engineering*, stanford University, Stanford, California.

Moeck, I. (2013), Classification of geothermal plays according to geological habitats, in *IGA Academy Report; Geothermal Exploration Best Practices – Geology, Exploration Drilling, Geochemistry, Geophysics*, vol. 1, edited by R. Bracke, C. Harvey, and H. Rueter, IGA Service GmbH, Bochum, Germany.

Moeck, I. (2014), Catalog of geothermal play types based on geological controls, *Renewable and Sustainable Energy Reviews*, *37*, 867–882.

Muñoz, G. (2014), Exploring for geothermal resources with electromagnetic methods, *Surveys in Geophysics*, *35*, 101–122.

Muñoz, G., K. Bauer, I. Moeck, A. Schulze, and O. Ritter (2010), Exploring the großschönebeck (germany) geothermal site using a statistical joint interpretation of magnetotelluric and seismic topography models, *Geothermics*, *39*, 35–45.

Newman, G., E. Gasperikova, G. Hoversten, and P. Wannamaker (2008), Three-dimensional magnetotelluric characterization of the coso geothermal field, *Geothermics*, *37*, 369–399.

Pellerin, L., J. Johnston, and G. Hohmann (1996), A numerical evaluation of electromagnetic methods in geothermal exploration, *Geophysics*, *61*(1), 121–130.

Rikitake, T. (1948), Note on the electromagnetic induction within the earth, *Bull. Earthq. Res. Inst., Univ. Tokyo*, *24*, 1–9.

Siripunvaraporn, W., G. Egbert, Y. Lenbury, and M. Uyeshima (2005), Three-dimensional magnetotelluric inversion: data-space method, *Physics of the Earth and Planetary Interiors*, *150*, 3–14.

Spichak, V. (2009), Electromagnetic sounding of geothermal zones, *Journal of Applied Geophysics*, *68*(4), 459–478.

Sternberg, B., J. Washburne, and L. Pellerin (1988), Correction for the static shift in magnetotellurics using transient electromagnetic soundings, *Geophysics*, *53*, 1459–1468.

Tikhonov, A. (1950), On determining electrical characteristics of the deep layers of the earth's crust, *Doklady*, *73*, 295–297.

Unsworth, M., W. Soyer, V. Tuncer, A. Wagner, and D. Barnes (2007), Hydrogeologic assessment of the amchitka island nuclear test site (alaska) with magnetotellurics, *Geophysics*, *72*(3), B47–B57.

van Leeuwen, W. (2016), *Working title:* geothermal exploration using the magnetotelluric method, Ph.D. thesis, Utrecht University, Faculty of Geosciences.

Wannamaker, P., R. P.E., D. W.M., J. McCulloch, and N. K. (2005), Magnetotelluric surveying and monitoring at the coso geothermal area, california, in support of the enhanced geothermal systems concept: Survey parameters, initial results, in *Proceedings World Geothermal Congress 2005*, Antalya, Turkey.

Williams, C., M. Reed, and A. A.F. (2011), Updating the classification of geothermal resources, in *Proceedings 36th workshop on geothermal reservoir engineering*, Stanford, CA: Stanford University.